Quantitative evaluation of catalytic effect on the desorption reaction of hydrogen storage materials on the basis of atomization energy concept

HIROSHI HIRATE

Nagoya University

January 2010

Content

Chapter 1 General Introduction

Nowadays, total energy calculation is so common in the field of material science. However, information of the chemical bond between atoms is still limited along the total energy calculation alone.

In 1955, Wigner and Seitz [1] predicted that if one had a great calculating machine, one might apply it to the problem of solving the Schrödinger equation for each metal and thereby obtain values for their physical quantities, such as the cohesive energy and the lattice constant. It is not clear, however, that a great deal would be gained by this. Presumably, the results would agree with experimentally determined quantities and nothing vastly new would be learned from the calculation. This prediction, made by two pioneers of solid-state physics, still appears to be true today, even though computational science has made great progress.

In addition, the Mulliken population analysis [2] is very common in the field of molecular orbital calculation, and the nature of the chemical bond between atoms has been defined well using the standard concept of covalent and ionic bonds. However, with this analysis it is still difficult to compare quantitatively the chemical bond strengths among a variety of materials, because, both covalent and ionic interactions are operating in most of materials. To solve this problem, the chemical bond should be estimated quantitatively in an energy scale.

Recently, Nakai has proposed a new analyzing technique called energy density analysis (EDA) [3]. In this method, the total energy of a system, computed by the Kohn-Sham-type density functional theory (DFT) [4], is partitioned into atomic energy

densities, and the characteristics of the chemical bond are understood in terms of each atomic energy density instead of the total energy. Shinzato et al. have applied this method to the analysis of the chemical bond between atoms in various hydrides and hydrocarbons [5-7]. In this analysis, the atomization energy for each constituent atom is newly defined by subtracting the atomic energy density from the total energy of the isolated atom. This analysis allows us to compare the nature of the chemical bond between atoms among a variety of materials in a quantitative way. For example, the cohesive energy is expressed as the sum of the atomization energies of every element in the material, so the role of each element in the chemical bond formation is understood readily using the atomization energies.

In this study, this theoretical approach using the atomization energy is applied to the catalytic reaction problem of hydrogen storage materials.

In the field of hydrogen storage materials, many kinds of the hydrides such as metal hydrides [8-10] and complex hydrides [11, 12] have been investigated as shown in Fig. 1-1. However, there are still several barriers to practical use of them for the on-board application. For example, metal compounds such as $LaNi_5$ and TiFe absorb hydrogen at room temperature to form metal hydrides, $LaNi_5H_6$ and $TiFeH_2$, but their hydrogen capacities are very limited. On the other hand, complex hydrides being composed of light elements (e.g., AlH_3, $NaAlH_4$ and $LiBH_4$) possess a high hydrogen capacity, but their hydrogenation and dehydrogenation reaction rates are very slow.

In 1997, Bogdanović and Schwickardi [11] and Liang et al. [13] reported that some metals and metal compounds have remarkable catalytic effects on the hydrogen desorption reaction of several hydrides. Since then, various metal compounds have been

investigated for use of catalysts on the desorption reaction of hydrogen storage materials, for example, metal oxide catalysts accelerate the desorption reaction of magnesium hydride [14] and metal chloride catalysts enhance the decomposition reaction of alkali metal (= Na) and alkaline earth metal (= Mg, Ca) alanates [11, 15]. However, the mechanism for the catalytic effect of these catalysts on these reactions still remains unknown, and no quantitative approach has been proposed yet. Such as quantitative approach to the catalytic effect is indeed needed to find more effective catalysts.

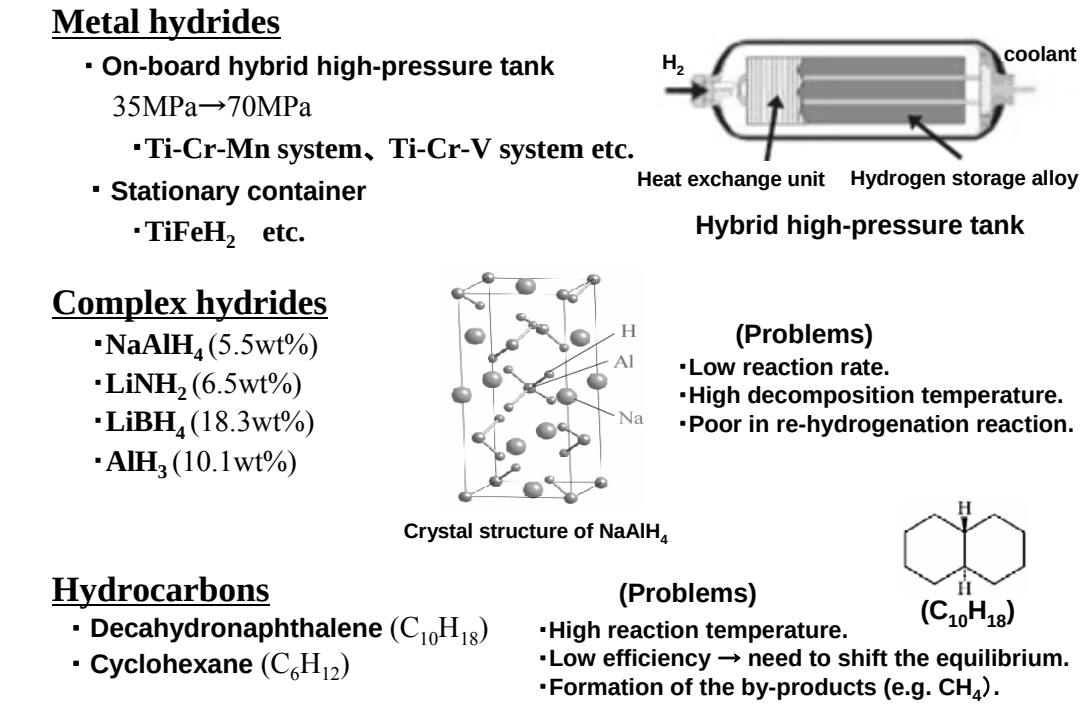

Fig. 1-1. Current status of hydrogen storage materials.

In general, it is thought that metal site and anion site in binary metal compound work individually as a catalytic site on the catalytic reaction. For example, magnetite (Fe_3O_4) is an ammonia synthesized catalyst discovered by Mittash [16]. It is considered that the reduced Fe atoms work on the dissociation and adsorption reaction of N_2, and O

atoms weaken the Fe-N bond and enhance the desorption of NH_3 on a Fe catalyst surface [17]. Thus, it is expected that quantitative evaluation of various catalysts becomes possible if the role of each constituent element can be estimated properly. We would be able to understand the catalytic effect of metal compounds quantitatively by calculating the energy of each constituent element following the atomization energy concept.

The purpose of this study is to evaluate quantitatively the catalytic effect of metal oxides and metal chlorides on the hydrogen desorption reaction of MgH_2 and $NaAlH_4$ using atomization energy. For this purpose, the crystal structures of metal oxides and chlorides are optimized by plane-wave pseudopotential method [18] in order to clarify the stable structure. Then total energy calculation is performed using Gaussian03, and it is partitioned into the atomic energy densities for constituent elements by using EDA. The advantage of using atomization energy is to know the contribution of each constituent element to the oxide or chloride formation. The atomization energy is a unique quantity that can never be obtained from the total energy calculation alone.

Following the research background and the purpose as mentioned earlier, this paper is composed of six Chapters. The outline of each chapter is given below.

In Chapter 1, the problem of the total energy calculation and the Mulliken population analysis and the possibility of using atomization energy concept on the catalytic problem are explained together with the principal purpose of this study.

In Chapter 2, two calculation methods used in the present study are explained. One is the plane-wave pseudopotential method and the other is the energy density analysis (EDA) method.

In Chapter 3, quantitative approach based on the atomization energy concept is proposed for understanding the catalytic effect of metal oxides on the hydrogen desorption reaction of MgH_2.

In Chapter 4, to confirm the presence of the O-H interaction during the course of hydrogen desorption reaction of MgH_2, the O-H vibration mode in Nb_2O_5-catalyzed MgH_2 is examined experimentally using FT-IR spectroscopy.

In Chapter 5, following the atomization energy concept, the catalytic effect of metal chlorides is understood quantitatively on the hydrogen decomposition reaction of $NaAlH_4$.

In Chapter 6, a general conclusion obtained from this study is summarized.

REFERENCES

[1] E. P. Wigner and F. Seitz, Solid State Phys. 1 (1955) 97-126.

[2] R. S. Mulliken, J. Chem. Phys. 23 (1953) 1833-1840.

[3] H. Nakai, Chem. Phys. Lett. 363 (2002) 73-79.

[4] W. Kohn and L. J. Sham, Phys. Rev. 140 (1965) A1133-1138.

[5] Y. Shinzato, H. Yukawa, M. Morinaga, T. Baba and H. Nakai, J. Alloys Compd. 446 (2007) 96-100.

[6] Y. Shinzato, H. Yukawa, M. Morinaga, T. Baba and H. Nakai, Acta Mater. 55 (2007) 6673-6680.

[7] Y. Shinzato, H. Yukawa, M. Morinaga, T. Baba and H. Nakai, Adv. Quantum Chem. 54 (2008) 145-160.

[8] J. J. Reilly and R. H. Wiswall Jr, Inorg. Chem. 13 (1974) 218-222.

[9] H. H. Van Mal, K. H. J. Buschow and A. R. Miedema, J. Less-Common Met. 35 (1974) 65-76.

[10] D. L. Cummings and G. J. Powers, Ind. Eng. Chem., Process Des. Develop. 13 (1974) 182-192.

[11] B. Bogdanović and M. Schwickardi, J. Alloys Compd. 253-254 (1997) 1-9.

[12] A. Züttel, P. Wenger, S. Rentsch, P. Sudan, Ph. Mauron and Ch. Emmenegger, J. Power Sources 118 (2003) 1-7.

[13] G. Liang, J. Huot, S. Boily, A. Van Neste and R. Schulz, J. Alloys Compd. 292 (1999) 247-252.

[14] G. Barkhordarian, T. Klassen and R. Bormann, J. Phys. Chem. B 110 (2006) 11020-11024.

[15] K. Komiya, N. Morisaku, Y. Shinzato, K. Ikeda, S. Orimo, Y. Ohki, K. Tatsumi, H. Yukawa and M. Morinaga, J. Alloys Compd. 446-447 (2007) 237-241.

[16] A. Mittasch, E. Keunecke, Z. Elektrochem. 38 (1932) 666-669.

[17] M. S. Spencer, Catal. Lett. 13 (1992) 45-54.

[18] V. Milman, B. Winkler, J. A. White, C. J. Pickard, M. C. Payne, E. V. Akhmatsukaya and R. H. Nodes, Int. J. Quant. Chem. 77 (2000) 895-910.

Chapter 2 Calculation Methods

2.1 Calculation Methods

Geometry optimizations are employed using the first principles plane-wave pseudopotential (PW-PP) technique [1].

The main idea of PW-PP is to simplify the DFT problem by considering only valence electrons. Core electrons are excluded under the assumption that the charge densities of core electrons are not affected by any changes in the chemical environment. This approximation is well understood and it gives several advantages over DFT calculations:

- The pseudopotential is much weaker in the core region than the true Coulomb potential of the nucleus, and it does not have a singularity at the position of the nucleus.
- The resulting pseudo-wave functions are smooth and nodeless in the core region.
- Both pseudopotentials and pseudo-wave functions can be efficiently represented using a plane-wave basis set.
- Relativistic effects, which are mainly due to core electrons, can be included in the pseudopotential.
- There are fewer electronic states in the solid-state calculation.

In the present PW-PP calculations, the effective electron-electron interaction is treated within the generalized gradient approximation (GGA) expressed as the Perdew-Wang form [2, 3]. The Vanderbilt's ultrasoft pseudopotentials are employed in the calculation [4]. The ultrasoft pseudopotential has great advantage in both accuracy

and computational cost for elements with the valence 1s, 2p, 3d or 4f electrons where the norm-conserving potentials are necessarily hard [1].

The coupling with PW-PP and state-of-the-art computation for the iterative minimization of the total energy enables us to perform efficient and accurate geometry optimization [1]. For the electronic structure calculation, the self-consistent total energy in the ground state is obtained effectively by the density-mixing scheme [1, 5]. The geometry of those complex solid state materials which contain more than 10 degrees of freedom as atomic internal coordinates and cell parameters is optimized using the quasi-Newton method with the Broyden-Fletcher-Goldfarb-Shanno (BFGS) algorithm [6].

The plane-wave basis size and the number of **k**-points using for the Brillouin zone integration should be sufficiently large with respect to the accuracy needed for the purpose of the study. The former is usually set by the kinetic energy cutoff of the plane-waves. The **k**-points are chosen according to the mesh generated by Monkhorst and Pack's scheme [7].

2.2 Energy density analysis (EDA)

The electronic structures for optimized crystal lattice of hydrides are obtained by the DFT calculations under the periodic boundary condition (PBC) using the Gaussian03 program package (Gaussian, Inc., Wallingford, CT). The adopted functional is the BLYP functional, which consists of the Slater exchange [8], the Becke (B88) exchange [9], the Vosko-Wilk-Nusair correlation [10] and the Lee-Yang-Parr correlation functionals [11]. In this study, the EDA calculations under PBC [12] are

performed by linking the original code for the EDA with the Gaussian03.

Following the EDA, the atomic energy density of A atom is evaluated by,

$$E^{\mathrm{A}} = E^{\mathrm{A}}_{\mathrm{NN}} + E^{\mathrm{A}}_{\mathrm{KIN}} + E^{\mathrm{A}}_{\mathrm{Ne}} + E^{\mathrm{A}}_{\mathrm{CLB}} + E^{\mathrm{A}}_{\mathrm{XC}} \quad , \tag{1}$$

where $E^{\mathrm{A}}_{\mathrm{NN}}$ is the nuclear-nuclear repulsion energy density, $E^{\mathrm{A}}_{\mathrm{KIN}}$ is the non-interacting kinetic energy density, $E^{\mathrm{A}}_{\mathrm{Ne}}$ is the nuclear-electron attraction energy density, $E^{\mathrm{A}}_{\mathrm{CLB}}$ is the Coulomb energy density, $E^{\mathrm{A}}_{\mathrm{XC}}$ is the exchange-correlation energy density.

In equation (1), for example, $E^{\mathrm{A}}_{\mathrm{XC}}$, is evaluated by the partial sum for the numerical quadrature technique,

$$E^{\mathrm{A}}_{\mathrm{XC}} = \sum_{g}^{grid} \varpi_g \, p_g(r_g) F_{\mathrm{XC}}(r_g) \quad , \tag{2}$$

where ϖ_g is the weighting factor, $p_g(r_g)$ is the partition function, and $F_{\mathrm{XC}}(r_g)$ is the exchange-correlation functional. The other terms in equation (1), which are evaluated by the analytical integration with the Kohn-Sham orbitals, are partitioned into their energy densities on the analogy of Mulliken population analysis [13]. For example, the Coulomb energy density for atom A, $E^{\mathrm{A}}_{\mathrm{CLB}}$, is evaluated by,

$$E^{\mathrm{A}}_{\mathrm{CLB}} = \frac{1}{2} \sum_{\mu \in \mathrm{A}} (PG)_{\mu\mu} \quad , \tag{3}$$

where $\boldsymbol{P}$ is the atomic orbital-basis density matrix and the element of $\boldsymbol{G}$ is given by

$$G_{\nu\mu} = \sum_{\lambda} \sum_{\sigma} P_{\lambda\sigma} \left\langle \chi_\nu \chi_\mu \middle| \chi_\sigma \chi_\lambda \right\rangle \quad . \tag{4}$$

Further detailed explanation of the calculation is given elsewhere [12, 14].

2.3 Atomization energy

In this section, the calculation method of atomization energy is explained using as example of metal oxide. The EDA analysis is performed with the geometry optimized by the plane-wave pseudopotential method. For binary metal oxide, M*x*O*y*, the respective atomic energy densities of M and O are related closely to the nature of the chemical bond relevant to M and O atoms in M*x*O*y*. When the energy of the isolated neutral atom, $E_{\mathrm{M}}^{\mathrm{atom}}$ (or $E_{\mathrm{O}}^{\mathrm{atom}}$), is taken as a reference, the atomization energy, ΔE_{M} (or ΔE_{O}), is defined as,

$$\Delta E_{\mathrm{M}} = \left(E_{\mathrm{M}}^{\mathrm{atom}} - E_{\mathrm{M}}^{\mathrm{oxide}}\right) \times \left(x/y\right) \quad , \tag{5}$$

$$\Delta E_{\mathrm{O}} = \left(E_{\mathrm{O}}^{\mathrm{atom}} - E_{\mathrm{O}}^{\mathrm{oxide}}\right) \quad , \tag{6}$$

where $E_{\mathrm{M}}^{\mathrm{oxide}}$ and $E_{\mathrm{O}}^{\mathrm{oxide}}$ are the atomic energy densities for M and O in M*x*O*y*, respectively. In the above equation (5), a coefficient, (*x*/*y*), is multiplied to $\left(E_{\mathrm{M}}^{\mathrm{atom}} - E_{\mathrm{M}}^{\mathrm{oxide}}\right)$, so this ΔE_{M} is the average energy partitioned into M to be counted per oxide ion.

Then, the cohesive energy, E_{coh}, of the oxide per oxide ion is defined as,

$$E_{\mathrm{coh}} = \Delta E_{\mathrm{M}} + \Delta E_{\mathrm{O}} \, . \tag{7}$$

Thus, ΔE_{M} and ΔE_{O} are the components of E_{coh}. A relation between cohesive energy and atomization energies is illustrated in Fig. 2-1 for monoxide, MO. Each of the atomization energies become a measure of the chemical bonding effect of the element on the formation of the metal oxide, MO.

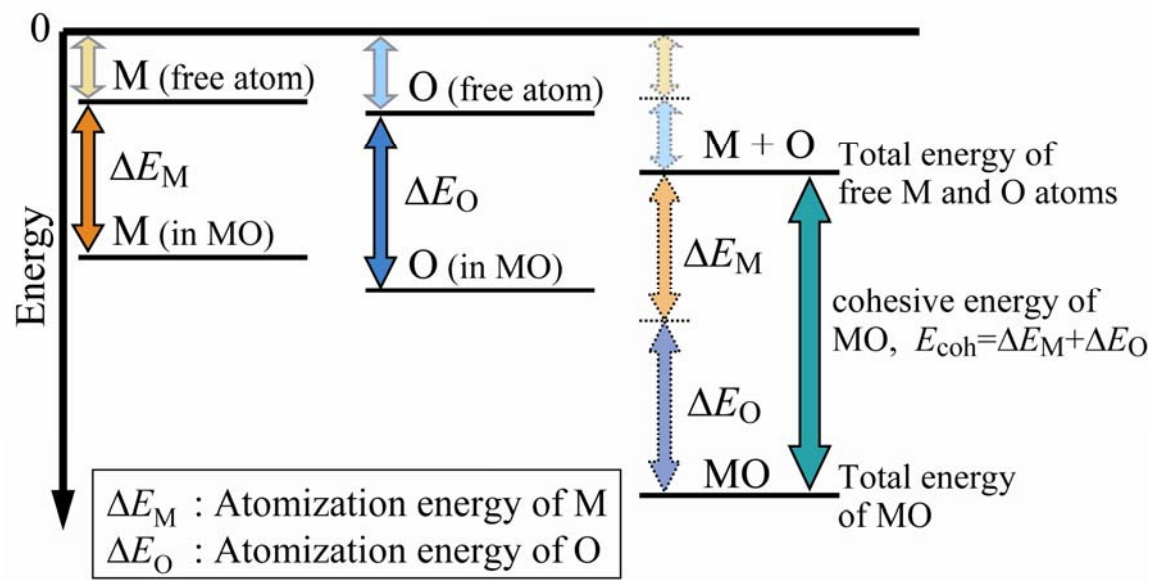

Fig. 2-1. Schematic illustration of cohesive energy and atomization energies for MO.

The element with the higher atomization energy contributes more significantly to the oxide formation than the other element, and provides an active site for the chemical reaction. On the other hand, the element with the lower atomization energy behaves as if it is a non-reactive element. For example, as explained in Chapter 3, ΔE_O is higher than ΔE_M in any transition-metal based oxides. As a result, the oxide ion in the metal oxide catalyst interacts more strongly with hydrogen than the metal ion during the course of dehydrogenation reaction of MgH_2.

REFERENCES

[1] V. Milman, B. Winkler, J. A. White, C. J. Pickard, M. C. Payne, E. V. Akhmatskaya and R. H. Nobes, Int. J. Quant. Chem. 77 (2000) 895-910.

[2] J. P. Perdew, K. Burke and Y. Wand, Phys. Rev. B 54 (1996) 16533-16539.

[3] J. P. Perdew, J. A. Chevary, S. H. Vosko, K. A. Jackson, M. R. Pederson, D. J. Singh and C. Fiolhais, Phys. Rev. B 46 (1992) 6671-6687.

[4] D. Vanderbilt, Phys. Rev. B 41 (1990) 7892-7895.

[5] G. Kresse and J. Furthmüller, Phys. Rev. B 54 (1996) 11169-11186.

[6] S. A. Teukolsky, W. T. Vetterling and B. P. Flannery, Numerical Recipes 2nd ed., W. H. Press, New York, 1992.

[7] H. J. Monkhorst and J. D. Pack, Phys. Rev. B 13 (1976) 5188-5192.

[8] J. C. Slater, Phys. Rev. 81 (1951) 385-390.

[9] A. D. Becke, Phys. Rev. A 38 (1988) 3098-3100.

[10] S. H. Vosko, L. Wilk and M. Nusair, Can. J. Phys. 58 (1980) 1200-1211.

[11] C. Lee, W. Yang and R. G. Parr, Phys, Rev. B 37 (1988) 785-789.

[12] H. Nakai, Y. Kurabayashi, M. Katouda and T. Atsumi, Chem. Phys. Lett. 438 (2007) 132-138.

[13] R. S. Mulliken, J. Chem. Phys. 23 (1955) 1833-1840.

[14] H. Nakai, Chem. Phys. Lett. 363 (2002) 73-79.

Chapter 3 Quantitative Approach to the Understanding of Catalytic Effect of Metal Oxides on the Desorption Reaction of MgH_2 using the Atomization Energy

3.1 Introduction

As mentioned in Chapter 1, the catalytic reactions have been investigated in the field of hydrogen storage material. In particular, there are a large number of reports on the metal oxide catalysts for the hydrogen desorption reaction of magnesium hydride (MgH_2).

MgH_2 has been considered as one of the promising hydrogen storage materials because it possesses a high hydrogen capacity of 7.6 mass%. However, the heat of formation of MgH_2, ΔH, is -74 kJ/mol H_2 [1, 2], indicating that MgH_2 is a relatively stable hydride. As a result, the rate of the desorption reaction, i.e., $MgH_2 \rightarrow Mg + H_2$, is slow in the moderate conditions. In 1999, Liang et al. presented a result that some metals act as a catalyst to enhance the hydrogen absorption and desorption reactions [3]. Also, it has been reported that transition metal oxides (e.g., Fe_3O_4, Nb_2O_5) have a high catalytic effect on the hydrogen desorption reaction of MgH_2 [4- 7]. In recent years, the catalytic mechanism has been investigated extensively in MgH_2 [7- 11]. For example, Barkhordarian et al. reported the change in the hydrogen desorption reaction rate with catalytic metal oxides as shown in Fig. 3-1 (a) for 1 mol % oxide mixing [7] and (b) for 0.2 mol % oxide mixing [5]. In either case, Nb_2O_5 is the most effective catalyst among the oxides. The catalytic data of Fe_3O_4 is also shown in Fig. 3-1 (b).

In addition, the hydrogen absorption kinetics was investigated for MgH_2 catalyzed

by Nb_2O_5 [8] and the valence state of Nb ion in the mixed Nb_2O_5 was shown to be less than 5+, due to the occurrence of partial reduction by hydrogen atoms in MgH_2 during the catalytic reaction [9].

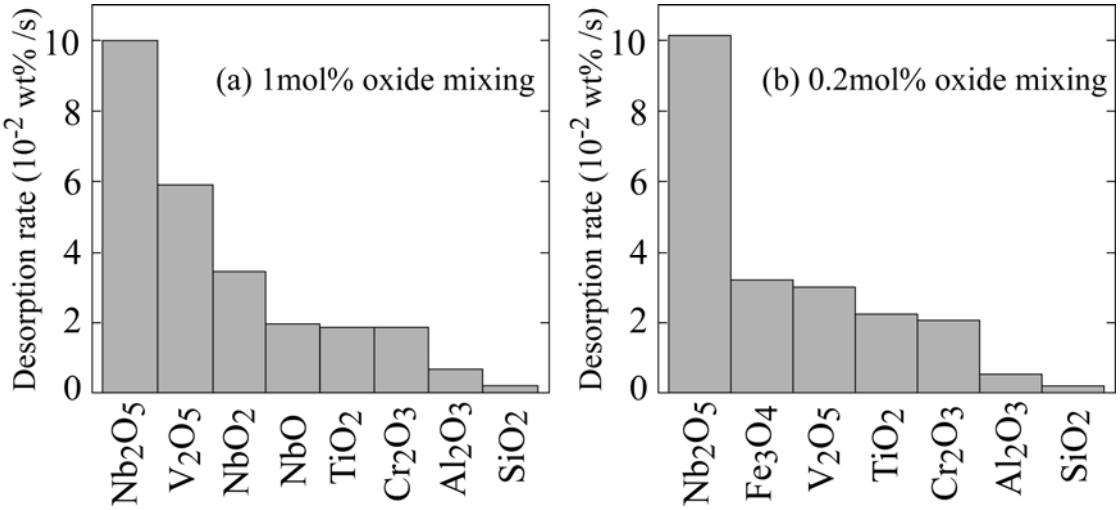

Fig. 3-1. Various metal oxides and their catalytic effect on hydrogen desorption reaction rate of MgH_2 at 573K; (a): left figure for 1 mol % oxide mixing, (b): right figure for 0.2 mol % mixing.

In this chapter, atomization energy concept is applied to the understanding of catalytic reaction of metal oxides on the desorption reaction of MgH_2. For this purpose, the atomization energies of constituent elements in metal oxides are first calculated and used to understand quantitatively the catalytic effect of metal oxides on the hydrogen desorption reaction of MgH_2.

3.2 Calculation procedure

3.2.1 Geometry optimization

The crystal structures of metal oxides are optimized by the total energy minimization using the plane-wave pseudopotential method. For this purpose, the first-principle calculations based the density functional theory (DFT) are performed

with the generalized gradient approximation of Perdew et al. [12]. The implementation of DFT employed here combines a plane-wave basis set with the total energy pseudopotential method, as embodied in the CASTEP code [13]. The present calculations are based upon the ultrasoft pseudopotentials proposed by Vanderbilt [14]. The plane-wave cutoff energy is chosen to be 380 eV. The sampling in the reciprocal space is done with *k*-point grids, e.g., $6\times6\times4$ for monoclinic Nb_2O_5.

3.2.2 EDA calculation and atomization energy

The electronic structures for optimized crystal lattice of metal oxides are obtained by the DFT calculations under the periodic boundary condition (PBC) using Gaussian03 program package (Gaussian, Inc., Wallingford, CT). The adopted functional is the BLYP functional [15]. The following modified Gaussian basis sets are adopted: (i) the Ahlrichs pVDZ [16] basis set without the outer s function and constructed to be double zeta class for Fe, (ii) the Huzinaga basis sets [17] without the outer s function and constructed to be double zeta class for V, Cr and Nb, (iii) the 6-31G basis sets [18, 19] for O and without the outer s function for Al and Ti, (iv) the Ahlrichs TZV basis set without the outer s and p functions for K and Si [20], (v) the correlation-consistent polarization plus the valence double zeta (pVDZ) basis sets of Dunning [21, 22] without p-type functions for H, and without the d-type functions for Mg. In this study, the EDA calculations under PBC [23] are performed by linking the original code for the EDA with Gaussian03. Further detailed explanation of the EDA calculation is given elsewhere [23, 24]

For binary metal oxides, M*x*O*y*, the atomization energy, ΔE_M (or ΔE_O), is defined

as in chapter 2,

$$\Delta E_{\mathrm{M}} = \left(E_{\mathrm{M}}^{\mathrm{atom}} - E_{\mathrm{M}}^{\mathrm{oxide}}\right) \times (x/y) \ , \qquad (1)$$

$$\Delta E_{\mathrm{O}} = \left(E_{\mathrm{O}}^{\mathrm{atom}} - E_{\mathrm{O}}^{\mathrm{oxide}}\right) \ . \qquad (2)$$

In the above equation (1), a coefficient, (x/y), is multiplied to $\left(E_{\mathrm{M}}^{\mathrm{atom}} - E_{\mathrm{M}}^{\mathrm{oxide}}\right)$, so this ΔE_{M} is the average energy partitioned into M to be counted per oxide ion.

Then, the cohesive energy, E_{coh}, of the oxide per oxide ion is defined as,

$$E_{\mathrm{coh}} = \Delta E_{\mathrm{M}} + \Delta E_{\mathrm{O}} \ . \qquad (3)$$

Thus, ΔE_{M} and ΔE_{O} are the components of E_{coh}. By setting $Y = \Delta E_{\mathrm{O}}$ and $X = \Delta E_{\mathrm{M}}$, we obtain a relation, $Y = -X + E_{\mathrm{coh}}$. So, E_{coh} is expressed as a point of intersection of this line and the Y-axis at $X = 0$.

3.3 Results and Discussion

3.3.1 Cohesive energy for binary metal oxides

Table 3-1. Calculated and experimental cohesive energies for metal oxides. (units: eV)

	E_{coh}(Calc.)	E_{coh}(Exp.)		E_{coh}(Calc.)	E_{coh}(Exp.)
Al_2O_3	10.67	10.59	Fe_3O_4	8.41	8.71
SiO_2	9.49	9.63	NbO	15.35	14.38
TiO_2	10.23	9.92	NbO_2	10.14	10.51
V_2O_5	8.44	7.94	Nb_2O_5	9.31	9.56
Cr_2O_3	9.19	9.27	K_2O	7.90	8.21

The cohesive energy, E_{coh}, is a measure of the electronic stability of any oxides. As shown in Table 3-1, the difference between the calculated and experimental values [25] for E_{coh} lies within 0.5 eV, except for NbO, in which both cation and anion vacancies are arranged to form an ordered defect structure [26]. Thus, the present calculation is

performed in a reasonable manner.

3.3.2 Atomization energy diagram for binary metal oxides

The plots of ΔE_M vs. ΔE_O, are shown in Fig. 3-2 for binary metal oxides, M*x*O*y*. This ΔE_M vs. ΔE_O diagram is called “atomization energy diagram”. According to Eq. (3), those oxides which are located in the upper right region in this figure, have large cohesive energies. Also, the contribution of each element in the oxide to the cohesive energy is understood from this figure.

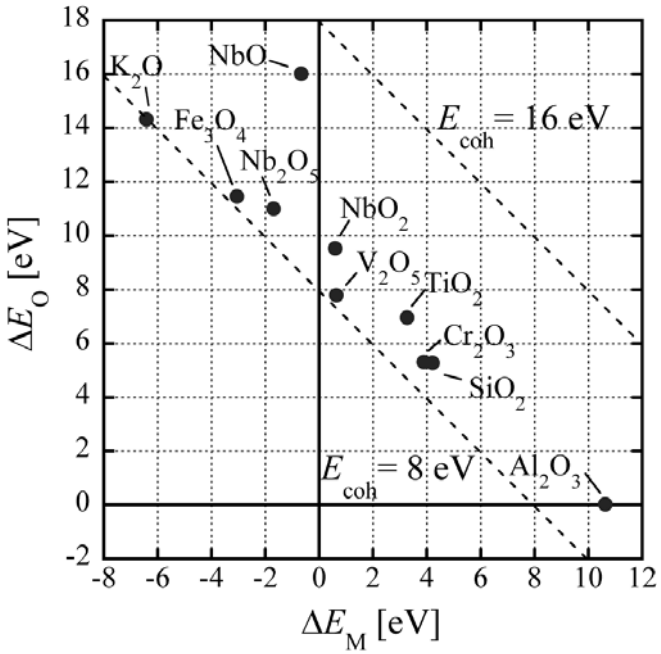

Fig. 3-2. Atomization energy diagram for metal oxide catalysts.

For example, the cohesive energy is nearly same between NbO_2 and Al_2O_3 (NbO_2: E_{coh} =10.1 eV, Al_2O_3: E_{coh} =10.7 eV). However, they are located in the very different positions in Fig. 3-2. NbO_2 has a large ΔE_O value, but a very small ΔE_M value, indicating that the oxide ions in NbO_2 make a significant contribution to the cohesive energy. On the other hand, in case of Al_2O_3, the value of ΔE_O is almost zero. Instead, its

ΔE_M value is very large. This indicates that the metal ions in Al_2O_3 contribute mainly to the cohesive energy. In this way, using the atomization energy diagram, the roles of each constituent element in the stability of metal oxides can be understood in a straightforward manner. Such information is, however, never obtained from the total energy calculation alone.

3.3.3 Quantitative analysis of catalytic effect of metal oxides using the atomization energies

As mentioned before, metal oxides possess a catalytic effect on the hydrogen desorption reaction of MgH_2. Shown in Fig. 3-1 (a) and (b) are the experimental data reported by Barkhordarian et al. [5, 7]. Thus, the catalytic effect is highest in Nb_2O_5, followed by V_2O_5. But, the catalytic effect of Fe_3O_4 may be slightly superior to V_2O_5, judging from Fig. 3-1 (b). Therefore, it is conceivable that catalytic effects of metal oxides change in the order, $Nb_2O_5 > Fe_3O_4 > V_2O_5 > NbO_2 > NbO > TiO_2 > Cr_2O_3 > Al_2O_3 > SiO_2$. It is evident that transition metal oxides are better catalysts than non-transition metal oxides (e.g., Al_2O_3, SiO_2).

To understand this catalytic effect quantitatively, the atomization energies of constituent elements in metal oxides are used, and the results are shown in Fig. 3-3 for $y \times \Delta E_M$ and in Fig. 3-4 for $y \times \Delta E_O$. In each figure, (a) is the result for 1mol% oxide mixing and (b) is the result for 0.2 mol% oxide mixing.

As is evident from Eqs. (1) and (2), ΔE_M and ΔE_O are defined as the values per oxide ion. However, metal oxides, M*x*O*y*, are mixed by a mole unit in the experiments. So, we need to convert the values of the atomization energies per oxide ion into the

values per mole unit to compare them with the experimental data. So, each of ΔE_M and ΔE_O are multiplied by the number of oxide ions, y, in MxOy. The atomization energy to be counted per mole unit is expressed as $y \times \Delta E_M$ for metal ions and $y \times \Delta E_O$ for oxide ions, since $y \times \Delta E_M = \left(E_M^{atom} - E_M^{oxide}\right) \times x$ and $y \times \Delta E_O = \left(E_O^{atom} - E_O^{oxide}\right) \times y$, following the Eqs. (1) and (2).

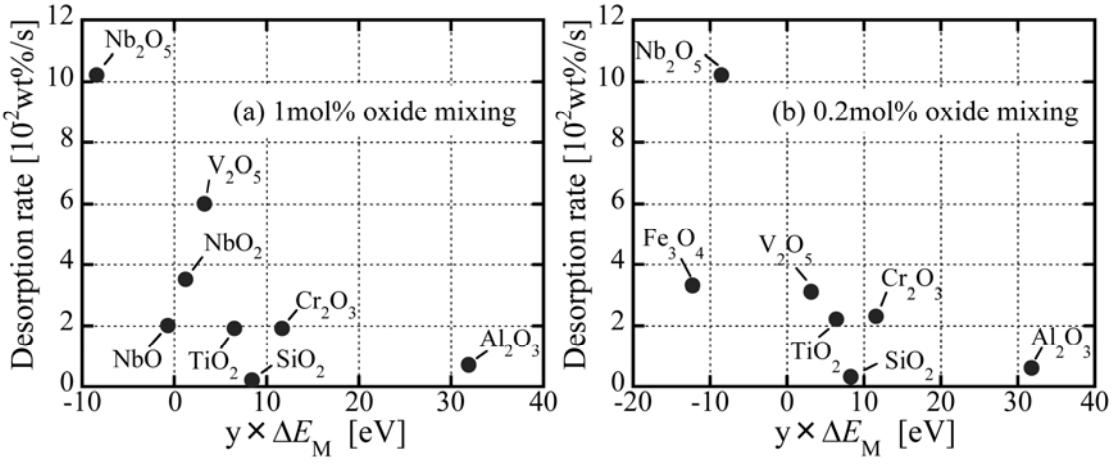

Fig. 3-3. $y \times \Delta E_M$ vs. desorption rate of MgH_2 with metal oxide catalysts; (a): 1 mol% oxide mixing, (b): 0.2 mol% oxide mixing.

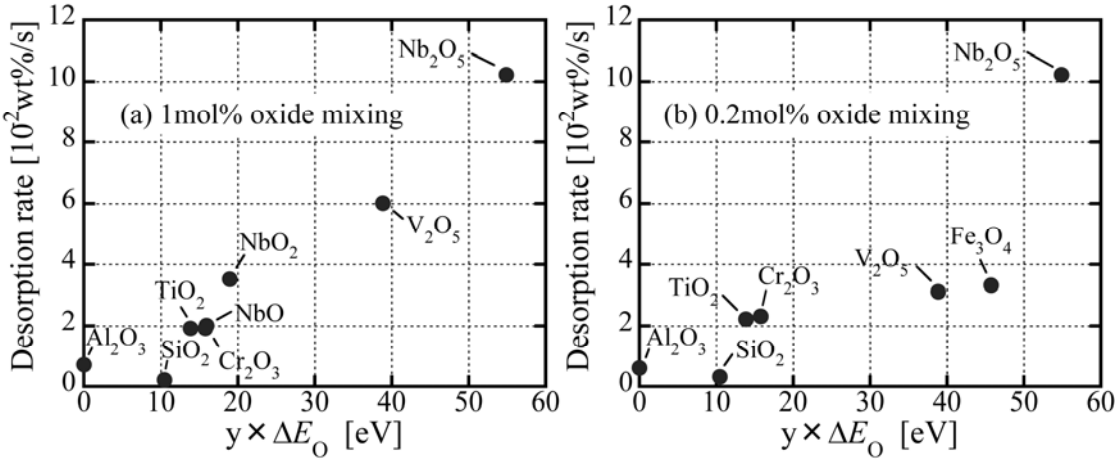

Fig. 3-4. $y \times \Delta E_O$ vs. desorption rate of MgH_2 with metal oxide catalysts; (a): 1 mol% oxide mixing, (b): 0.2 mol% oxide mixing.

(A) *Correlation with atomization energy of metal ion*

As shown in Fig. 3-3 (a) and (b), the data are scattered, but still there is a certain

trend that the mixing of those metal oxides which have the small values of $y \times \Delta E_M$, accelerates the rate of hydrogen desorption reaction in MgH_2. This means that the M atom with the smaller atomization energy interacts more strongly with hydrogen atom during the catalytic reaction.

However, this trend disagrees with our previous result of the atomization energy to be observed in the course of the hydrogen absorption reaction of TiFe compound, i.e., $TiFe + H_2 \rightarrow TiFeH_2$ [27]. It is well known that hydrogen atom interacts more strongly with Fe atom than Ti atom in TiFe compound, and H atom occupies the position near Fe atom in the crystal structure of $TiFeH_2$. According to the calculation [27], the atomization energy of Fe is much larger than that of Ti in TiFe compound [27]. In other words, the Fe atom with the higher atomization energy atom interacts preferably with hydrogen atom to form a $TiFeH_2$. In this process, most of the Fe energy is transferred to hydrogen atom, resulting in the high atomization energy of H in $TiFeH_2$. Thus, it is considered that the higher atomization-energy atom provides more active sites for hydrogen atom. The same trend is also observed in another hydrogen absorption reaction of Mg_2Ni compound, i.e., $Mg_2Ni + 2H_2 \rightarrow Mg_2NiH_4$ [27]. In this case, Ni atom with the higher atomization energy interacts with hydrogen atom to form a Mg_2NiH_4. The energy transfer from Ni atom to the hydrogen atom also occurs in this hydrogen absorption process.

On the analogy of this, the element that interacts more strongly with hydrogen atom in MgH_2 must be the element with the higher atomization energy in the metal oxide. In the present case, it is not the metal ion, but the oxide ion, as shown in Fig. 3-2. An exception is seen in Al_2O_3, where the atomization energy is higher in Al than in O.

In such a case, catalytic effect is very weak probably due to the very weak interaction operating between O and H atoms.

(B) *Correlation with atomization energy of oxide ion*

On the other hand, as shown in Fig. 3-4 (a) and (b), the mixing of those metal oxides which have large values of $y \times \Delta E_O$ tends to accelerate the rate of hydrogen desorption reaction in MgH_2. The oxide ions in the metal oxides with larger $y \times \Delta E_O$ values are supposed to interact more strongly with hydrogen atoms in MgH_2. Such an O-H interaction between M*x*O*y* and MgH_2 gives a beneficial effect on the catalytic reaction. In this sense, $y \times \Delta E_O$ is a measure of the catalytic effect of metal oxides, M*x*O*y*.

The presence of such a strong O-H interaction may be verified by the calculated results of the atomization energies in MgH_2, where ΔE_H = 2.96 eV and ΔE_{Mg} = 0.38 eV that is a value to be counted per hydrogen atom [27]. This ΔE_H is higher than the ΔE_H value of 2.24 eV for H_2 molecule, but its ΔE_{Mg} is lower than the ΔE_{Mg} value of 0.76 eV for Mg metal. Here, the cohesive energy of Mg metal is 1.51 eV, and its half value is defined as ΔE_{Mg} for comparison. It is clear that the hydrogen state is stabilized in MgH_2. As a result, the hydrogen atom with the higher atomization energy in MgH_2 tends to interact mainly with the oxide ion in metal oxides, as explained above. However, it still remains unknown what transition state is formed by this O-H interaction in the desorption process of MgH_2.

3.3.4 Comparison with previous models

Barkhordarian et al. [7] investigated experimentally a catalytic mechanism of transition-metal oxides (or compounds) on the Mg hydrogen desorption reaction. Four factors were proposed for the transition-metal oxide to be an effective catalyst: (i) a large number of structural defects; (ii) a low stability of the oxide, which, however, has to be high enough to avoid complete reduction of the transition-metal ion under operating conditions; (iii) a high valence state of the transition-metal ion in the oxide; (iv) a high affinity of the transition-metal ion to hydrogen.

Their model appears to be made on the basis of the idea that the transition-metal ion rather than the oxide ion interacts more strongly with hydrogen atom in MgH_2. However, the experimental result that Fe_3O_4 has a relatively high catalytic effect, as shown in Fig. 3-1 (b), contradicts the factor (iv). This is because, the interaction between Fe and hydrogen atom is weak. On the other hand, the value of $y \times \Delta E_O$ for Fe_3O_4 (45.8 eV) is intermediate between V_2O_5 (38.9 eV) and Nb_2O_5 (55.0 eV), in agreement with the experiment shown in Fig. 3-4 (b). In addition, the factor (ii) may be important to some extent, but the catalytic activity of metal oxides changes in the order, $Nb_2O_5 > Fe_3O_4 > V_2O_5 > NbO_2 > NbO > TiO_2 > Cr_2O_3 > Al_2O_3 > SiO_2$, which is very different from the order of the cohesive energy, $NbO > Al_2O_3 > NbO_2 > TiO_2 > Nb_2O_5 > SiO_2 > Cr_2O_3 > Fe_3O_4 > V_2O_5$, as shown in Table 3-1.

The other two factors are probably important; although structural defect of the factor (i) is not treated in the present approach. In case of the factor (iii), a high valence state of the transition-metal ion in the oxide, M*x*O*y*, means that *y*/*x* is large, and hence a large value of $y \times \Delta E_O$ is expected in such an oxide.

3.3.5 Elemental processes of the desorption reaction in MgH_2 with metal oxide catalyst

The hydrogen desorption from MgH_2 is considered to be a combination of several elemental processes such as the decomposition reaction in the solid, $MgH_2 \rightarrow Mg + 2H$, the diffusion of hydrogen atom to surface and the recombination of hydrogen atoms to form a H_2 molecule. According to the desorption experiment of Nb_2O_5-mixed MgH_2 by Barkhordarian et al. [7, 28], the desorption kinetics of hydrogen is controlled either by chemisorption (recombination of hydrogen atoms) or by the moving velocity of the Mg/MgH_2 interface. The different mechanisms operate depending on the amount of Nb_2O_5 catalyst and on the milling time for preparing a mixture of MgH_2 and Nb_2O_5. Following their results, Nb_2O_5 catalyst is effective in facilitating the chemisorption behavior.

As described earlier, there is a strong O-H interaction operating between Nb_2O_5 and MgH_2. This interaction may facilitate not only the decomposition reaction in the solid, $MgH_2 \rightarrow Mg + 2H$, but also the chemisorption (recombination of hydrogen atoms) as discussed by Barkhordarian et al. [7, 28]. As ΔE_H = 2.24 eV in H_2, the hydrogen energy is recovered to some extent by the H_2 formation, as compared to the initial ΔE_H value of 2.96 eV in MgH_2. For metal catalysts other than Nb_2O_5, no experiments have been carried out to examine the elemental processes. However, it is supposed that most of them work in a similar manner as does Nb_2O_5.

In addition, as a result of the O-H interaction between M*x*O*y* and MgH_2, a certain transition state will appear in the course of hydrogen desorption reaction. For example, in case of Nb_2O_5 catalyst, a partially reduced niobium oxide phase and a mixed

Nb-Mg-O phase will be formed during the desorption [9, 29].

3.3.6 Application of the present approach to some other catalytic process

Concerning the oxide catalyst, there is a famous Haber-Bosch process [30] to synthesize ammonia, $N_2 + 3H_2 \rightarrow 2NH_3$. In this process, a mixture of Fe_3O_4, Al_2O_3 and K_2O is used as a catalyst. Fe_3O_4 has a good catalytic effect on this hydrogen absorption and dissociation reaction, and Al_2O_3 has a function to prevent sintering of Fe_3O_4 in this process without showing any catalytic effect [30]. These catalytic activities of Fe_3O_4 and Al_2O_3 in the synthesis process of ammonia are very similar to the results on the hydrogen desorption reaction of MgH_2, as shown in Fig. 3-4 (b). In addition, the $y \times \Delta E_O$ value for K_2O is about 14.3 eV, so judging for Fig. 3-4 (a) or (b), its catalytic effect is very small. Instead, it is said that K_2O has a function to keep the (111) surface of Fe_3O_4 active for the catalytic reaction [31] or to enhance the desorption of NH_3 from catalyst surface [32].

3.4 Conclusion

In order to understand the catalytic effect of metal oxides on the hydrogen desorption reaction of MgH_2, the atomization energies, ΔE_M for the metal ion and ΔE_O for the oxide ion are evaluated in various metal oxides, M*x*O*y*. It is found that the hydrogen desorption rate increases monotonously with increasing $y \times \Delta E_O$ values of metal oxides. The oxide ion in M*x*O*y* interacts mainly with hydrogen atom in MgH_2, and the catalytic reaction is enhanced through the O-H interaction between them. The present approach based on the atomization energy concept is applicable to various problems of catalytic reactions.

REFERENCE

[1] J. F. Stampfer Jr, C. E. Holley Jr and J. F. Suttle, J. Am. Chem. Soc. 82 (1960) 3504-3508.

[2] D. L. Cummings and G. J. Powers, Ind. Eng. Chem., Process Des. Develop. 13 (1974) 182-192.

[3] G. Liang, J. Huot, S. Boily, A. Van Neste and R. Schulz, J. Alloys Compd. 292 (1999) 247-252.

[4] W. Oelerich, T. Klassem and R. Bormann, J. Alloys Compd. 315 (2001) 237-242.

[5] G. Barkhordarian, T. Klassen and R. Bormann, Scr. Mater. 49 (2003) 213-217.

[6] G. Barkhordarian, T. Klassen and R. Bormann, J. Alloys Compd. 364 (2004) 242-246.

[7] G. Barkhordarian, T. Klassen and R. Bormann, J. Phys. Chem. B 110 (2006) 11020-11024.

[8] N. Hanada, T. Ichikawa and H. Fujii, J. Alloys Compd. 446-447 (2007) 67-71.

[9] F. Dolci, M. D. Chio and M. Baricco, J. Mater. Sci. 42 (2007) 7180-7185.

[10] A. Borgschulte, M. Bielmann, A. Züttel, G. Barkhordarian, M. Dornheim and R. Bormann, Appl. Surf. Sci. 254 (2008) 2377-2384.

[11] M. Porcu, A. K. Petford-Long and J. M. Sykes, J. Alloys Compd. 453 (2008) 341-346.

[12] JP. Perdew, K. Burke and Y. Wang, Phys. Rev. B 54 (1996) 16533-16539.

[13] V. Milman, B. Winkler, J. A. White, C. J. Pickard, M. C. Payne, E. V. Akhmatskaya and R. H. Noves, Int. J. Quant. Chem. 77 (2000) 895-910.

[14] D. Vanderbilt, Phys. Rev. B 41 (1990) 7892-7895

[15] J. C. Slater, Phys. Rev. 81 (1951) 385-390.

[16] A. Schafer, H. Horn and R. Ahlrichs, J. Chem. Phys. 97 (1992) 2571-2577.

[17] S. Huzinaga, J. Andzelm, M. Klobukowski, E. Radzioandzelm, Y. Sakai and H. Tatewaki, Gaussian Basis Sets for Molecular Calculation, Elsevier, New York, 1984.

[18] V. A. Rassolo, J. A. Pople, M. Ratner and T. L. Windus, J. Chem. Phys. 109 (1998) 1223-1229.

[19] W. J. Hehre, R. Ditchfield and J. A. Pople, J. Chem. Phys. 56 (1972) 2257-2261.

[20] A. Schafer, H. Horn and R. Ahlrichs, J. Chem. Phys. 100 (1994) 5829-5835.

[21] T. H. Dunning, J. Chem. Phys. 90 (1989) 1007-1023.

[22] D. E. Woon and T. H. Dunning, J. Chem. Phys. 98 (1993) 1358-1371.

[23] H. Nakai, Y. Kurabayashi, M. Katouda and T. Atsumi, Chem. Phys. Lett. 438 (2007) 132-138.

[24] H. Nakai, Chem. Phys. Lett. 363 (2002) 73-79.

[25] R. C. Weast, M. J. Astle and W. H. Beyer, CRC Handbook of Chemistry and Physics: A Ready-reference Book of Chemical and Physical Data (84th ed.), CRC Press, Boca Raton, 2003.

[26] A. L. Bowman, T. C. Wallace, J. L. Yarnell and R. G. Wenzel, Acta Crystallogr. 21 (1966) 843-843.

[27] Y. Shinzato, H. Yukawa, M. Morinaga, T. Baba and H. Nakai, Acta Mater. 55 (2007) 6673-6680.

[28] G. Barkhordarian, T. Klassen and R. Bormann, J. Alloys Compd. 407 (2006) 249-255.

[29] N. Hanada, T. Ichikawa and H. Fujii, Physica B 383 (2006) 49-50.

[30] A. Mittasch and E. Keunecke, Z. Elektrochem. 38 (1932) 666-669.

[31] S. K. Shaikhutdinov, W. Weiss and R. Schlögl, Appl. Surf. Sci. 161 (2000) 497-507.

[32] M. S. Spencer, Catal. Lett. 13 (1992) 45-54.

Chapter 4 Role of O-H Bonding in Catalytic Activity of Nb_2O_5 during the Course of Dehydrogenation of MgH_2

4.1 Introduction

The atomization energy concept was found to be useful for the quantitative estimation of the catalytic activities of metal oxides for the hydrogen desorption reaction of MgH_2 as explained in chapter 3. Here, the atomization energy concept will be explained briefly, because it is the purpose of this chapter to confirm this concept.

In chapter 3, a metal oxide expressed as M*x*O*y*, has the atomization energies $y \times \Delta E_M$ for M atoms and $y \times \Delta E_O$ for O atoms per molecular unit. According to a previous paper [1], the higher energy atom acts as the preferential reaction site. As O atom has the higher energy than M atom in most transition-metal oxides, the O atom is expected to act as such a reaction site in the oxide catalyst. So, $y \times \Delta E_O$ value for O atom was used as a measure of the catalytic activities of metal oxides. It was found that the measured hydrogen desorption rate of MgH_2 increases monotonously with increasing $y \times \Delta E_O$ values in M*x*O*y* as shown in Fig. 3-4 in chapter 3. This implies that the O atom in M*x*O*y* interacts mainly with H atom in MgH_2 during the hydrogen desorption. In other words, the O-H interaction is operating between them, resulting in the catalytic effect of metal oxides on the hydrogen desorption reaction of MgH_2.

The purpose of this chapter is to confirm the presence of the O-H interaction during the course of hydrogen desorption reaction of MgH_2. To this end, MgH_2 specimen catalyzed with Nb_2O_5 was prepared by ball milling, and the O-H vibration mode was searched for experimentally using FT-IR spectroscopy with the specimens on

the way to dehydrogenation.

4.2 Experimental procedure

4.2.1 Synthesis and dehydrogenation of MgH_2 with Nb_2O_5 catalyst

Powders of MgH_2 (98%) and Nb_2O_5 (99.99%) were purchased from Sigma-Aldrich Inc. The specimens were prepared from these powders by ball milling, using a planetary ball mill apparatus (Firitsch P7) where a weight ratio of stainless-steel balls to powders was set at 30:1. MgH_2 specimens with and without 1 mol% Nb_2O_5 catalyst were milled for 72 ks (20 hours) at 400 rpm under a hydrogen pressure of 1 MPa at ambient temperature. Also, only Nb_2O_5 or only MgH_2 was milled in the same way for comparison. In addition, non-milled Nb_2O_5 powder was supplied for the measurements of FT-IR and X-ray diffraction (XRD).

All the specimens were always handled in an argon-filled glove box equipped with a recirculation system to keep the water and oxygen concentrations below 1 ppm during operation.

For MgH_2 with 1 mol% Nb_2O_5, a hydrogen desorption curve was measured with holding time at 573 K in vacuum as shown in Fig. 4-1. This measurement was carried out by a standard volumetric method using a Sievert-type apparatus. On the basis of this result, four specimens were prepared for the FT-IR measurements. For the first specimen, hydrogen was not released by heating, and hereafter this is called non-released specimen that is located at the (A) point in Fig. 4-1. For the second specimen, hydrogen was released by about 2.3 wt% by heating the specimen for 250 seconds to reach the (B) point in Fig. 4-1, and hereafter this is called 2.3wt% released

specimen. For the third specimen, hydrogen was released by about 5.6 wt% by heating the specimen for 1000 seconds to reach the (C) point in Fig. 4-1, and this is called 5.6wt% released specimen. For the fourth specimen all the amount of hydrogen was released completely from MgH_2 by heating the specimen for a long time, 86.4ks (24hours) to reach the (D) point, and this is called all-released specimen. A theoretical amount of hydrogen all-released from MgH_2 is 7.6 wt%, but the measured value was about 6.9 wt%.

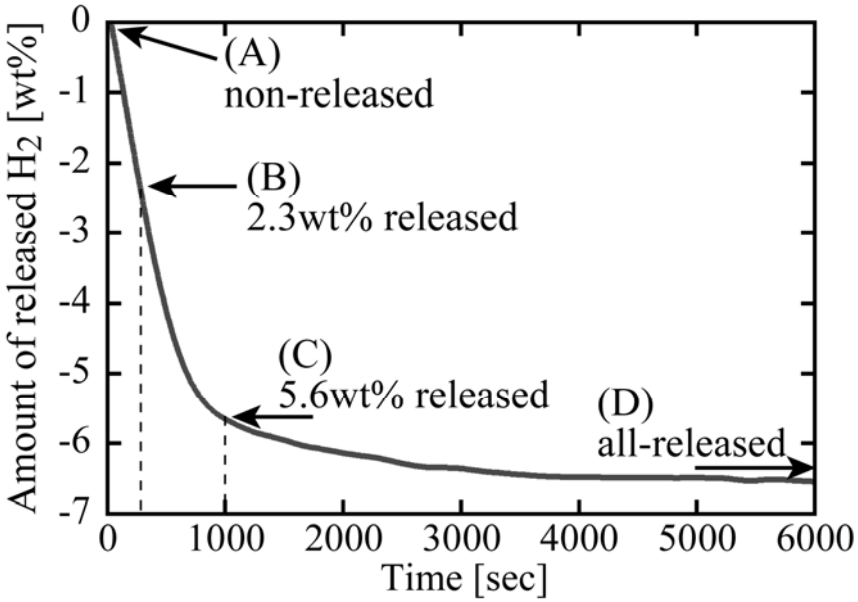

Fig. 4-1. Hydrogen desorption reaction curve measured at 573K in vacuum for MgH_2 with 1 mol% Nb_2O_5.

4.2.2 XRD and FT-IR measurements

X-ray powder diffraction patterns were taken by a Rigaku FR-E diffractmeter (Ni-filtered Cu-Kα radiation). Each specimen was filled into quartz glass capillary with 0.5 mm in diameter in a glove box. The capillary was sealed by the epoxy adhesive in a glove box to prevent the specimen from air.

Rather standard techniques were employed for the measurement of FT-IR spectroscopy. With the specimens prepared as potassium bromide (KBr) pellets, FT-IR spectra were measured in the range of 800 to 4000 cm^{-1} at room temperature in vacuum, using JASCO FT/IR-610 instrument.

4.3 Results and Discussion

4.3.1 X-ray diffraction patterns

The results of XRD measurements are shown in Fig. 4-2. As shown in Fig. 4-2 (a), a small amount of MgO was present in the milled MgH_2. MgO may be formed before or after milling due to the contamination of the specimen. Also, the XRD pattern of milled Nb_2O_5 shown in Fig. 4-2 (b) was the same as the pseudohexagonal one reported by Frevel et al [2]. However, this was very different from the XRD pattern of Nb_2O_5 shown in Fig. 4-2 (c). Partial reduction of Nb_2O_5 may occur by the milling under a hydrogen pressure of 1 MPa. As shown in Fig. 4-2 (d), such two types of Nb_2O_5 coexisted and MgO still remained in the non-released MgH_2-1mol% Nb_2O_5 specimen.

XRD patterns are shown in Fig. 4-2 (e) for 2.3wt% released specimen, (f) for 5.6wt% released specimen and (g) for all-released specimen. By comparing (d), (e), (f) and (g) with each other, it was apparent that the peak intensity of MgH_2 decreased but instead the peak intensity of Mg increased as the desorption reaction proceeded. In the all-released specimen there were no peaks from MgH_2, as might be expected from the complete release of hydrogen from the specimen. But the peak intensity of MgO retained nearly same in all these patterns. Also, peak intensities from two types of Nb_2O_5 around 23 degrees gradually decreased during desorption, but they appeared to

remain to some extent even in the all-released specimen shown in Fig. 4-2 (g). Thus, reduction of niobium oxide reported by Hanada [3] seemed to occur partially in these specimens during dehydrogenation, but it was never completed until Nb_2O_5 disappeared.

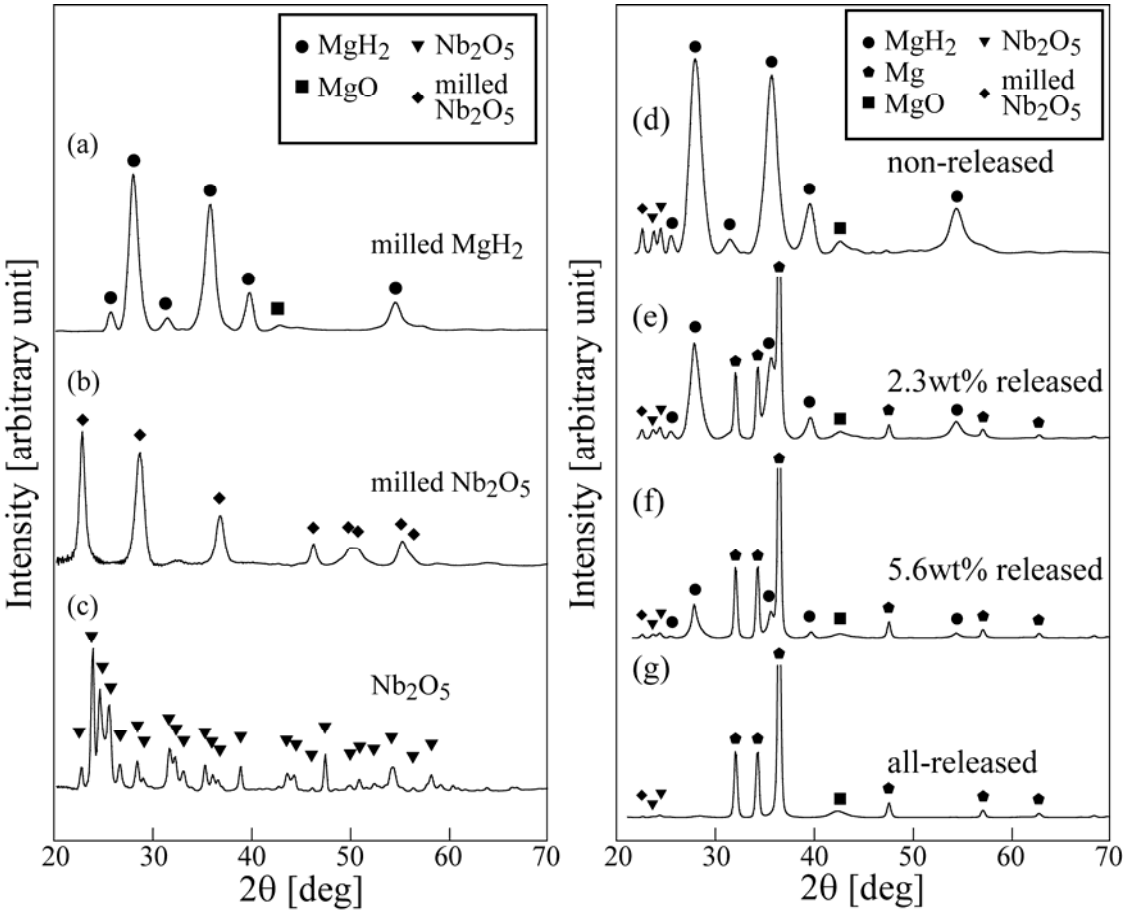

Fig. 4-2. XRD patterns of (a) milled MgH_2, (b) milled Nb_2O_5, (c) Nb_2O_5, and of MgH_2 with 1 mol% Nb_2O_5 where hydrogen was, (d) non-released (e) 2.3 wt% released, (f) 5.6 wt% released and (g) all-released.

4.3.2 FT-IR spectroscopy

(A) Absorption spectra in the region of 800 to 2000 cm^{-1}

The FT-IR spectra measured in the region of 800 to 2000 cm^{-1} are shown in Fig. 4-3 (a)~(e). In the spectrum of the non-released specimen shown in Fig. 4-3 (a), there are

two bands at 1010 and 1200 cm^{-1}, both of which were observed in the spectrum from milled MgH_2 as shown in Fig. 4-3 (e). These two bands nearly disappeared in the all-released specimens containing no MgH_2 as shown in Fig. 4-3 (d). So, they are attributable to the bands arising from MgH_2, probably assigned to the Mg-H bending mode. In addition, there was a band at 940 cm^{-1} in the non-released specimen, but it nearly disappeared in the other spectra of hydrogen-released specimens shown in Fig. 4-3 (b)~(d). But this band still remains unknown.

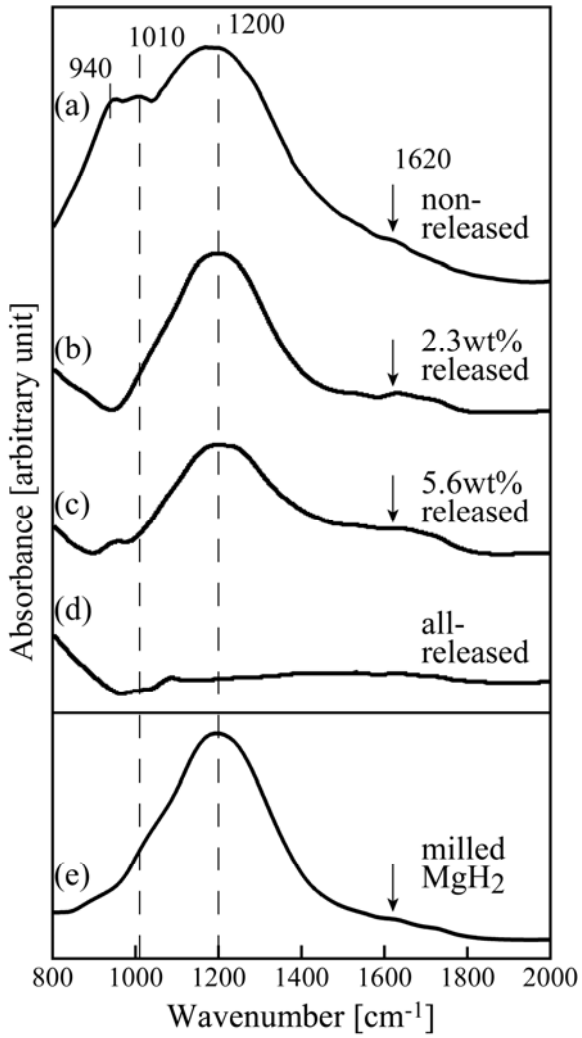

Fig. 4-3. FT-IR spectra of MgH_2 with 1 mol% Nb_2O_5 in the region of 800 to 2000 cm^{-1}, (a) non-released, (b) 2.3 wt% released, (c) 5.6 wt% released, (d) all-released specimen, and (e) milled MgH_2 for comparison.

When MgO is present, two bands at 1378 and 1463 cm^{-1} must appear in the spectrum following the SDBSWeb [4]. Neither band was, however, found in the spectra shown in Fig. 4-3 (a)~(e).

(B) Absorption spectra in the region of 2600 to 4000 cm^{-1}

Table 4-1. IR absorption frequency of O-H vibration in various substances.

Substance	Frequency	Vibrational mode	Reference
Nb_2O_5 - MgH_2	2800 ~ 3600 cm^{-1}	O-H stretching	present work
O-H in water	1600 ~ 1650 cm^{-1} 3200 ~ 3750 cm^{-1}	H-O-H bending O-H stretching	[5-8]
Nb-OH groups	3000 ~ 3800 cm^{-1}	O-H stretching	[9-12]
Nb_2O_5 - nH_2O	3640 ~ 3702 cm^{-1} 3000 ~ 3700 cm^{-1}	O-H stretching	[10]

Some of previous studies on the O-H vibration modes are summarized in Table 4-1. For example, the O-H bonding in water appears in the two regions of the absorption spectrum [5- 8]. One appears around 1600 ~ 1650 cm^{-1} due to the H-O-H bending mode and the other appears around 3200 ~ 3750 cm^{-1} due to the O-H stretching mode. On the other hand, the O-H bonding in the absorbed hydroxyl group appears in the region of 3000 ~ 3800 cm^{-1} due to the O-H stretching mode [9- 12]. In addition, the absorption spectrum of Nb_2O_5 surrounded by the coordinated H_2O (i.e., Nb_2O_5-nH_2O) is characteristic of the two bands at 3640 and 3702 cm^{-1} and the other broad band around 3000 ~ 3700 cm^{-1} [10]. Also, as discussed by Busca [9], the frequency of the O-H vibration depends on the O-H bond strength and also on the nature of the metal-O-H

bond, namely on the metal element to which the O-H is bonded. For example, the bands of the O-H bonding on Nb_2O_5 supported by TiO_2 appear at 3673, 3687 and 3720 cm^{-1}. Thus, most of the IR absorption frequencies due to the O-H vibration appear in the region of 3000 to 3800 cm^{-1}.

As shown in Fig. 4-4 (a), there were two bands at 3420 cm^{-1} and 3500 cm^{-1}, and a broad band from 2800 to 3300 cm^{-1} in the non-released specimen. The absorption intensities decreased gradually with decreasing amount of hydrogen retained in the specimen, as shown in Fig. 4-4 (a), (b) and (c). However, as shown in Fig. 4-4 (d), two small bands at 2880 cm^{-1} and 3450 cm^{-1} were still observed in the all-released specimen, despite that no MgH_2 existed, as explained in Fig. 4-4 (d). In addition, as shown in Fig. 4-4 (e), several bands appeared in the milled MgH_2, although the intensities were weaker compared to those of the non-released specimen shown in Fig. 4-4 (a). The band at 3450 cm^{-1} was also observed in the all-released specimen as shown in Fig. 4-4 (d). So, this may be related partially to the existence of MgO, since it was present in both the milled MgH_2 and all-released specimens as shown in Fig. 4-2 (a) and (g). Some O-H vibrations might retain on the surface of MgO, but the detail still remains unknown.

Two bands at 3420 cm^{-1} and 3500 cm^{-1} and a broad band in the region of 2800 to 3300 cm^{-1} were interpreted as due to the O-H stretching mode, following previous studies shown in Table 4-1. However, a portion of these bands might be still attributable to the O-H bonding in water on the specimen surface (see Table 4-1). In fact, as indicated by arrows in Fig. 4-3 (a)~(e), there was a very small hump around 1620 cm^{-1} due to the H-O-H bending mode in water [5-8]. However, the existence of water in the specimen was not detected in the experiment of thermal desorption mass spectroscopy.

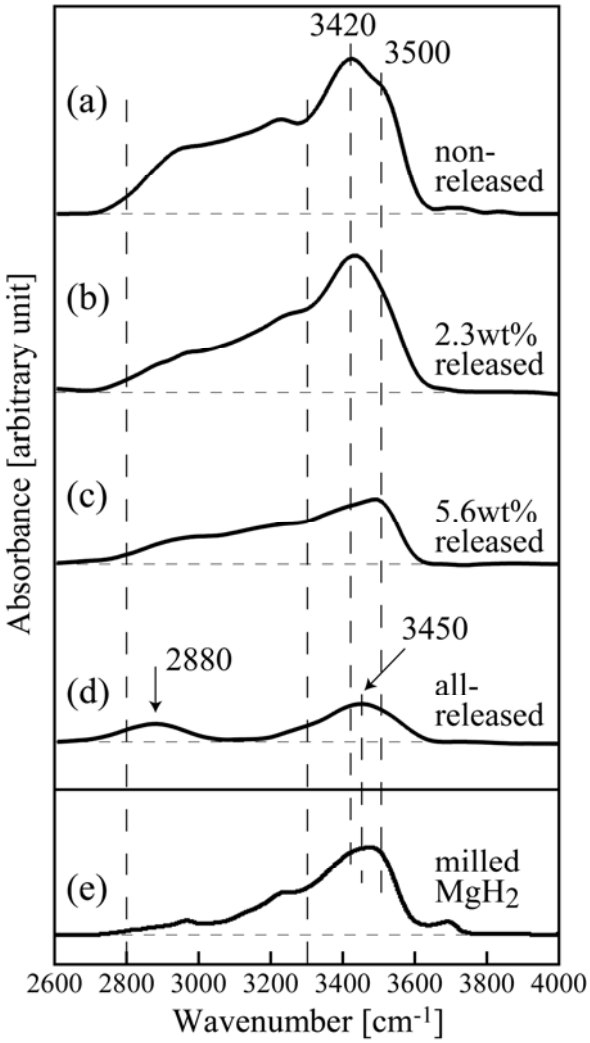

Fig. 4-4. FT-IR spectra of MgH_2 with 1 mol% Nb_2O_5 in the region of 2600 to 4000 cm^{-1}, (a) non-released, (b) 2.3 wt% released, (c) 5.6 wt% released, (d) all-released specimen, and (e) milled MgH_2 for comparison.

4.3.3 Existence of O-H interaction during dehydrogenation

Next, our attention was moved to the spectrum changes during dehydrogenation. Using the spectrum of the all-released specimen as a reference, each spectrum of non-released or partially released specimen was re-drawn in the region of 2600 to 4000 cm^{-1}. This was done simply by subtracting the spectrum data of the all-released specimen from each spectrum data of non-released or partially released specimen

presented in Fig. 4-4. The results are shown in Fig. 4-5 (a)~(c).

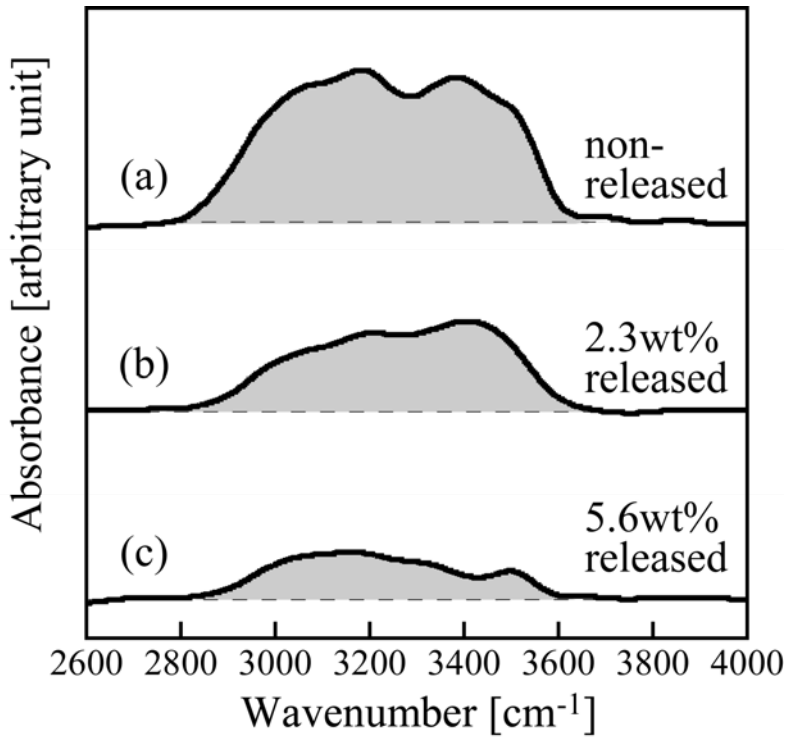

Fig. 4-5. Difference spectra of MgH_2 with 1 mol% Nb_2O_5 in the region of 2600 to 4000 cm^{-1}, (a) non-released, (b) 2.3wt% released and (c) 5.6wt% released specimen. These spectra shown in (a), (b) and (c) were obtained by subtracting spectrum data of all-released specimen from each spectrum data shown in Fig. 4-4 (a), (b) and (c), respectively.

It was apparent from this figure that the absorbance in the region of 2800 to 3600 cm^{-1} decreased monotonously with decreasing amount of hydrogen remained in the specimen during dehydrogenation. As shown in Fig. 4-6, the total area under the IR absorbance curve in the region of 2800 to 3600 cm^{-1} ,which was indicated by the shadow in the figure, was plotted against the amount of hydrogen remained in the specimen. The area of the non-released specimen containing about 6.9 wt% H_2 was used as a reference and set at 1.0 in the figure. The absorbance may be an indication of the amount of hydrogen remained in the specimen, since there was an approximately linear

relation between them. Thus, this spectrum change during dehydrogenation was considered as a direct evidence for the O-H stretching mode and hence for the existence of the O-H bonding at the surface of MgH_2 and Nb_2O_5 catalyst.

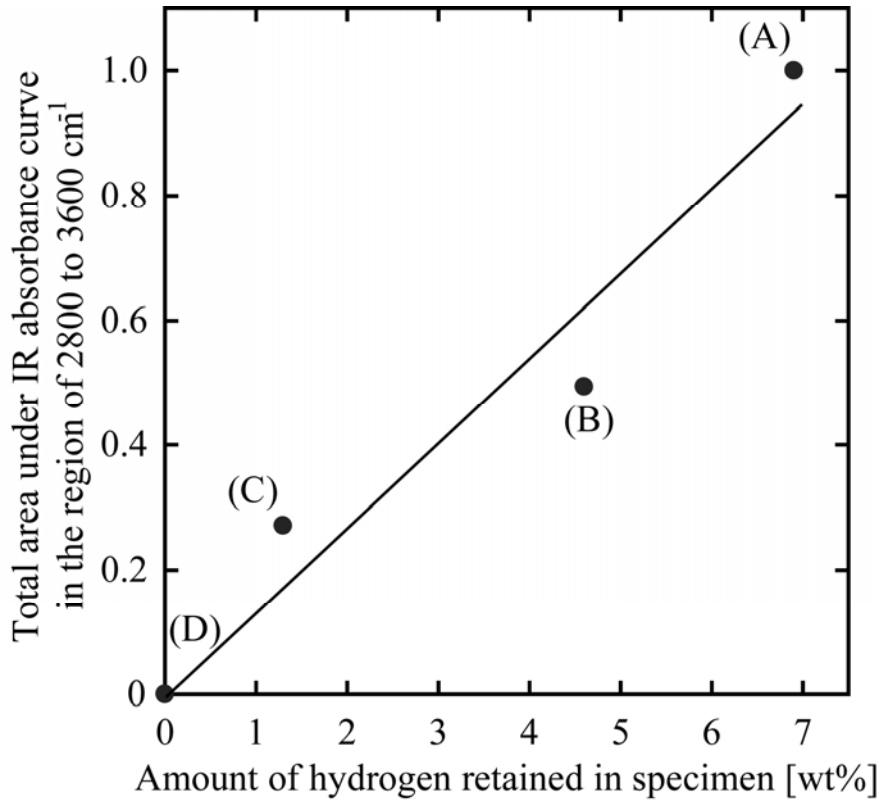

Fig. 4-6. Correlation between total area under IR absorbance curve in the region of 2800 to 3600 cm^{-1} and amount of hydrogen remained in specimen, (A) non-released, (B) 2.3wt% released, (C) 5.6wt% released and (D) all-released.

It was confirmed from the present experiment that the O-H interaction between Nb_2O_5 and MgH_2 is operating during the course of dehydrogenation of Nb_2O_5-catalyzed MgH_2. Therefore, the atomization energy of O atom, ΔE_O, in metal oxide catalysts is indeed a good measure of the catalytic activities in the hydrogen desorption reaction of MgH_2. Thus, the atomic energy concept is considered to be useful for the quantitative evaluation of catalytic activities in any chemical reactions.

4.4 Conclusion

The FT-IR spectra were measured with Nb_2O_5-catalyzed MgH_2 in order to confirm the presence of the O-H bonding between Nb_2O_5 and MgH_2 during the dehydrogenation. The absorption spectra due to the O-H stretching mode were observed experimentally in the region of 2800 to 3600 cm^{-1}, and the measured absorbance tended to decrease with decreasing amount of hydrogen in the specimen. The present experimental results supported strongly our previous analysis of the catalytic activities of metal oxides following the atomization energy concept.

REFERENCE

[1] Y. Shinzato, H. Yukawa, M. Morinaga, T. Baba and H. Nakai, Acta Mater. 55 (2007) 6673-6680.

[2] L. K. Frevel and H. W. Rinn, Anal. Chem. 27 (1955) 1329-1330.

[3] N. Hanada, T. Ichikawa and H. Fujii, H. Physica B 383 (2006) 49-50.

[4] http://riodb01.ibase.aist.go.jp/sdbs/ (National Institute of Advanced Industrial Science and Technology, 14 Sep 2009)

[5] M. V. Thiel, E. D. Becker and GC. Pimentel, J. Chem. Phys. 27(1957) 486-490.

[6] A. J. Tursi and E. R. Nixon, J. Chem. Phys. 52 (1970) 1521-1528.

[7] T. L. Tso and E. K. C. Lee, J. Phys. Chem. 89 (1985) 1612-1618.

[8] F. Franks, Water: a comprehensive treatise, vol.1, Plenum Press, New York, 1972.

[9] G. Busca, Catalysis Today 41 (1998) 191-206.

[10] L. J. Burcham, J. Datka and I. E. Wachs, J. Phys. Chem. B 103 (1999) 6015-6024.

[11] T. Armaroli, G. Busca, C. Carlini, M. Giuttari, A. M. R. Galletti and G. Sbrana, J. Mol. Catal. A-Chem. 151 (2000) 233-243.

[12] V. S. Braga, J. A. Dias, S. C. L. Dias and J. L. de Macedo, Chem. Mater. 17 (2005) 690-695.

Chapter 5 Quantitative Approach to the Understanding of Catalytic Effect of Metal Chlorides on the Decomposition Reaction of $NaAlH_4$ using the Atomization Energy

5.1 Introduction

In chapter 3, we evaluated quantitatively the catalytic effect of metal oxides (e.g., Nb_2O_5) on the hydrogen desorption reaction of MgH_2 by using the atomization energy. It is shown that the catalytic effect of metal oxides, M*x*O*y*, increases monotonously with increasing $y \times \Delta E_O$ values. The oxide ion in M*x*O*y* interacts mainly with hydrogen in MgH_2, and strong O-H interaction operates between them, resulting in the significant enhancement of the catalytic reaction of the hydrogen desorption. In this chapter, as another example, we focus on metal chloride catalysts for the decomposition reaction of sodium alanate ($NaAlH_4$).

Recently special attention has been directed toward complex hydrides, such as $NaAlH_4$, $LiNH_2$ and $LiBH_4$, because they are superior in both the gravimetric and volumetric densities of hydrogen to conventional hydrogen storage alloys. However, for these complex hydrides, there are still some problems in the reversibility of hydrogenation and dehydrogenation reactions, and also in high decomposition temperatures and low reaction rates. Bogdanović and Schwickardi first demonstrated that the doping of $TiCl_3$ catalyst enhances the kinetics and reversibility of hydrogen absorption and desorption reaction of $NaAlH_4$ [1]. $NaAlH_4$ releases hydrogen to form Na_3AlH_6 by the following reaction,

$$3NaAlH_4 \rightarrow Na_3AlH_6 + 2Al + 3H_2 \quad .$$

The enthalpy change, ΔH, of this reaction is about -37kJ/molH_2 and 3.7mass% H_2 is released at 373-393K [2]. Through this reaction, the four-coordinated complex anion, $[AlH_4]^-$ in $NaAlH_4$ transforms into the six-coordinated complex anion, $[AlH_6]^{3-}$ in Na_3AlH_6. Since Bogdanović and Schwickardi reported in 1997, extensive investigations have been made experimentally and theoretically on the catalytic effect on the hydrogen absorption and desorption reactions in various hydrides [3 - 11].

For example, Anton [3] has investigated catalytic effect of a variety of metal chlorides. A part of the results on the desorption rate change with chlorides are shown in Fig. 5-1, where (a) and (b) are the desorption rates measured in the time interval of 0-300 sec and 0-3600 sec after the desorption reaction starts, respectively.

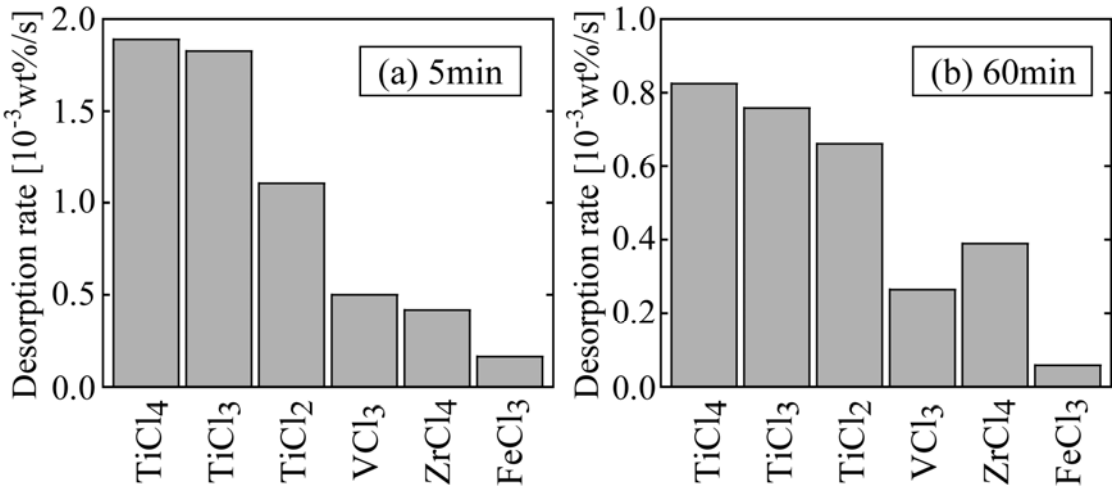

Fig. 5-1. Various metal chlorides and their catalytic effect on hydrogen desorption reaction rate of $NaAlH_4$ at 393K. Desorption rates are measured in the time interval of (a) 0-300sec, and (b) 0-3600 sec after desorption reaction starts.

In either case, $TiCl_4$ and $TiCl_3$ are very effective catalysts. Recently the study of the catalysts has been extended not only to chlorides, but also to other compounds including fluorides, oxides and lanthanides [4-7]. Among them, Ti chlorides of good catalysts have been investigated focusing on either the catalytic effect change with the mixing

content or the state change of the chlorides during the catalytic reaction [8]. By means of the XRD and EXAFS experiments, the Ti chloride is shown to be reduced in some ways, and the reduced Ti-dopant is in a very slightly oxidized or zerovalent state. In addition, it is shown that NaCl is formed in the specimen [9-11]. Such a reduced Ti dopant is supposed to work as the catalyst, although detailed mechanism for the catalytic reaction still remains unknown. No quantitative explanation has also been given for the catalytic effect of metal chlorides on the hydrogen desorption rate of $NaAlH_4$.

In this chapter, the atomization energy concept is applied to the catalytic reaction problem of $NaAlH_4$. For this purpose, the atomization energies of constituent elements in various metal chlorides are calculated and used to understand quantitatively the catalytic effect of metal chlorides on the decomposition reaction of $NaAlH_4$ to Na_3AlH_6. Also, to account for the Ti-state effect on the catalytic reaction, the hydrogen desorption rates are measured experimentally in $NaAlH_4$ mixed with Ti–based catalysts such as $TiCl_3$, TiO_2 and Ti metal nanopowder. In addition, hydrogen desorption temperature is measured with these specimens using thermal desorption mass spectroscopy (TDS).

5.2 Calculation procedure

5.2.1 Geometry optimization

In this study, the crystal structures of metal chlorides are optimized by the total energy minimization using the plane-wave pseudopotential method. $TiCl_4$ is liquid in room temperature (mp: 248K), so its crystal structure data at 150K [12] is used for the calculation. For this purpose, the first-principle calculations based the density functional

theory (DFT) are performed with the generalized gradient approximation of Perdew et al. [13]. The implementation of DFT employed here combines a plane-wave basis set with the total energy pseudopotential method, as embodied in the CASTEP code [14]. The present calculations are based upon the ultrasoft pseudopotentials proposed by Vanderbilt [15]. The plane-wave cutoff energy is chosen to be 380 eV. The sampling in the reciprocal space is done with *k*-point grids, e.g., $5\times5\times5$ for rhombohedral $TiCl_3$.

5.2.2 EDA calculation and atomization energy

The electronic structures for optimized crystal lattice of metal chlorides are obtained by the DFT calculations under the periodic boundary condition (PBC) using Gaussian03 program package (Gaussian, Inc., Wallingford, CT). The adopted functional is the BLYP functional [16]. The following modified Gaussian basis sets are adopted: (i) the Ahlrichs pVDZ [17] basis set for Cl and without the outer s function and constructed to be double zeta class for Fe, (ii) the Huzinaga basis sets [18] without the outer s function and constructed to be double zeta class for V and Zr, (iii) the 6-31G basis sets [19,20] without the outer s function for Ti, (iv) the correlation-consistent polarization plus the valence double zeta (pVDZ) basis sets of Dunning [21, 22] without p-type functions for H and without d-type functions for Na and Al. In this study, the EDA calculations under PBC [23] are performed by linking the original code for the EDA with Gaussian03.

For binary metal chlorides, MCl_n, the atomization energy, ΔE_M (or ΔE_{Cl}), is defined as in chapter 2,

$$\Delta E_M = \left(E_M^{atom} - E_M^{chloride}\right)/n \quad , \qquad (1)$$

$$\Delta E_{\mathrm{O}} = \left(E_{\mathrm{Cl}}^{\mathrm{atom}} - E_{\mathrm{Cl}}^{\mathrm{oxide}} \right) \ . \qquad (2)$$

In the above equation (1), $\left(E_{\mathrm{M}}^{\mathrm{atom}} - E_{\mathrm{M}}^{\mathrm{chloride}} \right)$ is divided by n, so this ΔE_{M} is the average energy of M to be counted per chloride ion. In this way, ΔE_{M} is defined as the normalized value per chloride ion, since n charges with the metal chlorides (e.g., n=4 for $TiCl_4$ and n=3 for $TiCl_3$).

Then, the cohesive energy, E_{coh}, of the chloride per chloride ion is expressed as,

$$E_{\mathrm{coh}} = \Delta E_{\mathrm{M}} + \Delta E_{\mathrm{Cl}} \ . \qquad (3)$$

Thus, ΔE_{M} and ΔE_{Cl} are the components of E_{coh}. By setting $Y = \Delta E_{\mathrm{Cl}}$ and $X = \Delta E_{\mathrm{M}}$, we obtain a relation, $Y = -X + E_{\mathrm{coh}}$. So, E_{coh} is expressed as a point of intersection of this line and the *Y*-axis at $X = 0$.

5.3 Experimental procedure

5.3.1 Purification and preparation for $NaAlH_4$

Powder of $NaAlH_4$ (90%) is purchased from Sigma-Aldrich Inc. The purified sample is prepared by the method mentioned in literature [24] and [25]. Namely, about 10 g of $NaAlH_4$ is dissolved into about 100 ml of dehydrated tetrahydrofuran (THF, less than 50 ppm H_2O) and then it is stirred for 3 hours (10.8 ks). The supernatant liquid of the mixture is decanted using a syringe and concentrated in vacuum to the volume of 20 ml. Then, 80 ml of dehydrated pentane (less than 10 ppm H_2O) is added to the THF solution to separate $NaAlH_4$ from the solution as a fine precipitate. The suspension is stirred for 1 hour (3.6 ks) and the supernatant liquid is removed on the instant. The precipitate is washed two times with pentane and dried in vacuum to obtain a fine white powder of $NaAlH_4$.

Doped catalysts into purified $NaAlH_4$ are 4 mol% $TiCl_3$, Ti nanopowders and TiO_2. The milling is performed in a planetary ball mill apparatus (Firitsch P7) at 400 rpm for 1.8 ks under a hydrogen pressure of 1.5 MPa at ambient temperature. Also, pure $NaAlH_4$ without catalyst is milled in the same way for comparison.

All the specimens are always handled in an argon-filled glove box equipped with a recirculation system to keep the water and oxygen concentrations below 1 ppm during operation.

5.3.2 Measurements of hydrogen desorption behavior in $NaAlH_4$ with and without catalyst

The hydrogen desorption temperatures of these specimens are measured using thermal desorption mass spectroscopy (TDS). The heating rate in the TDS measurement is set at 0.5K/min and the temperature is raised up to 773K in high vacuum by using a turbo-molecular pump. Also, for every specimen the hydrogen desorption reaction rate is measured at 393K by using PCT measurement system. Then, amounts of hydrogen gas desorbed from the specimen are measured accurately in a high-vacuum closed cell.

5.4 Results and Discussion

5.4.1 Cohesive energy for binary metal chlorides

The cohesive energy, E_{coh}, is a measure of the electronic stability of a chloride. As shown in Table 5-1, the difference between the calculated and experimental values [26] for E_{coh} lies within about 0.6 eV. Thus, the present calculation is performed in a reasonable manner.

Table 5-1. Calculated and experimental cohesive energies for metal chlorides (unit: eV).

	E_{coh}(Calc.)	E_{coh}(Exp.)		E_{coh}(Calc.)	E_{coh}(Exp.)
$TiCl_4$	4.78	4.70	VCl_3	4.55	5.18
$TiCl_3$	5.26	5.51	$FeCl_3$	3.76	4.21
$TiCl_2$	6.05	6.49	$ZrCl_4$	5.11	5.50

5.4.2 Atomization energy diagram for binary metal chlorides

The plots of ΔE_M vs. ΔE_{Cl} are shown in Fig. 5-2 for binary metal chlorides, MCl_n. This ΔE_M vs. ΔE_{Cl} diagram is called "atomization energy diagram". According to Eq. (3), those chlorides which are located in the upper right region in this figure, have large cohesive energies. Also, the contribution of each element in the chloride to the cohesive energy is understood from this figure. For example, the cohesive energy is nearly same between $TiCl_3$ and $ZrCl_4$ ($TiCl_3$: E_{coh} = 5.26 eV, $ZrCl_4$: E_{coh} = 5.11 eV). However, they are located in the very different positions in Fig. 5-2. $ZrCl_4$ has a large ΔE_{Cl} value, but a very small ΔE_M value, indicating that the chloride ions in $ZrCl_4$ make a significant contribution to the cohesive energy. On the other hand, in case of $TiCl_3$, the ratio of ΔE_M to ΔE_{Cl} value is about 0.86. This indicates that the metal ions as well as chloride ions contribute to the cohesive energy. Other transition metal chlorides shown in Fig. 5-2 show the same trend as $TiCl_3$, as ΔE_M is nearly equal to ΔE_{Cl}. For comparison, the result of NaCl is plotted in the figure, where ΔE_M is much larger than ΔE_{Cl}, being in contrast to the transition metal chlorides. In this way, using the atomization energy diagram, the role of each constituent element in the stability of metal chlorides can be understood in a straightforward manner. Such information is, however, never obtained from the total energy calculation alone.

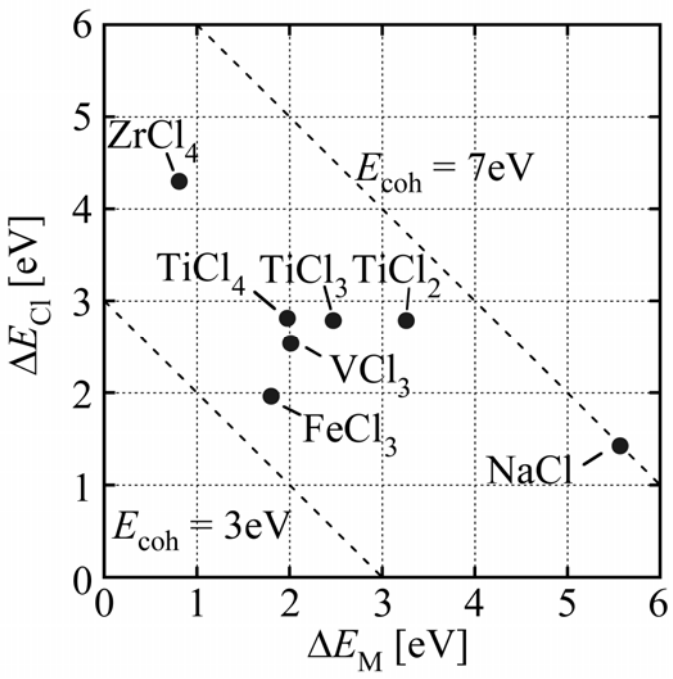

Fig. 5-2. Atomization energy diagram for metal chlorides.

5.4.3 Quantitative analysis of catalytic effect of metal chlorides using the atomization energies

As mentioned before, metal chlorides possess a catalytic effect on the hydrogen decomposition reaction of $NaAlH_4$ to Na_3AlH_6. Shown in Fig. 5-1 (a) and (b) are the experimental data reported by Anton [3]. Fig. 5-1 (a) is the result of the average initial desorption rate in the time interval of 0~5 min (0~300 sec) after the onset of the desorption reaction, of $NaAlH_4$ containing 2 mol% metal chloride. Fig. 5-1 (b) is the result of the average hydrogen desorption reaction rate measured in the later stage of desorption, i.e., 0~60 min (0~3600 sec) after the onset. Thus, judging from Figure 1 (b), the catalytic effect is highest in $TiCl_4$, and it changes in the order, $TiCl_4 > TiCl_3 > TiCl_2 > ZrCl_4 > VCl_3 > FeCl_3$, although the order of $ZrCl_4$ and VCl_3 is reverse in Fig. 5-1 (a).

To understand this catalytic effect quantitatively, the atomization energies of

constituent elements in metal chlorides are used, and the results are shown in Fig. 5-3 for $n \times \Delta E_M$ and in Fig. 5-4 for $n \times \Delta E_{Cl}$. In each figure, (a) is the result for hydrogen desorption reaction rate for 0-300 sec and (b) is the result for 0-3600 sec.

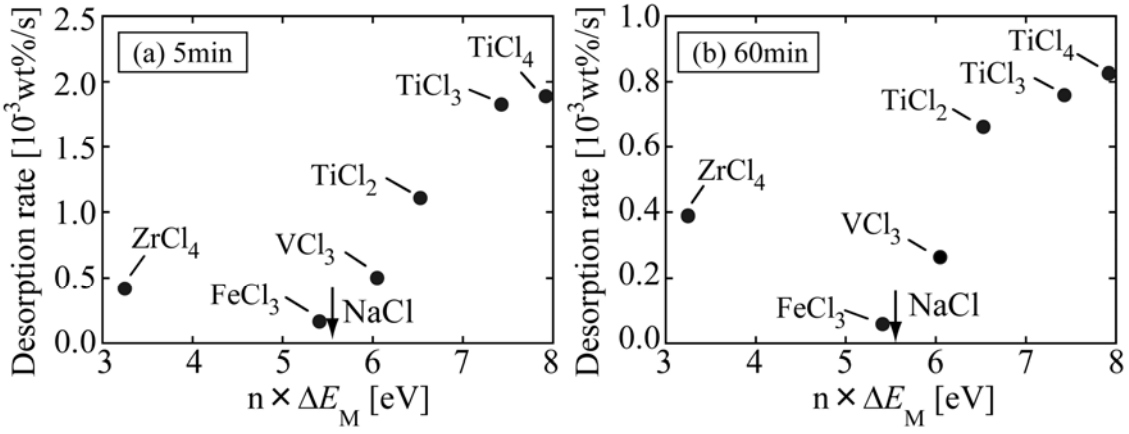

Fig. 5-3. $n \times \Delta E_M$ vs. desorption rate of $NaAlH_4$ with 2mol% metal chloride catalysts. Desorption rate is measured (a) for 0-300 sec and (b) for 0-3600 sec.

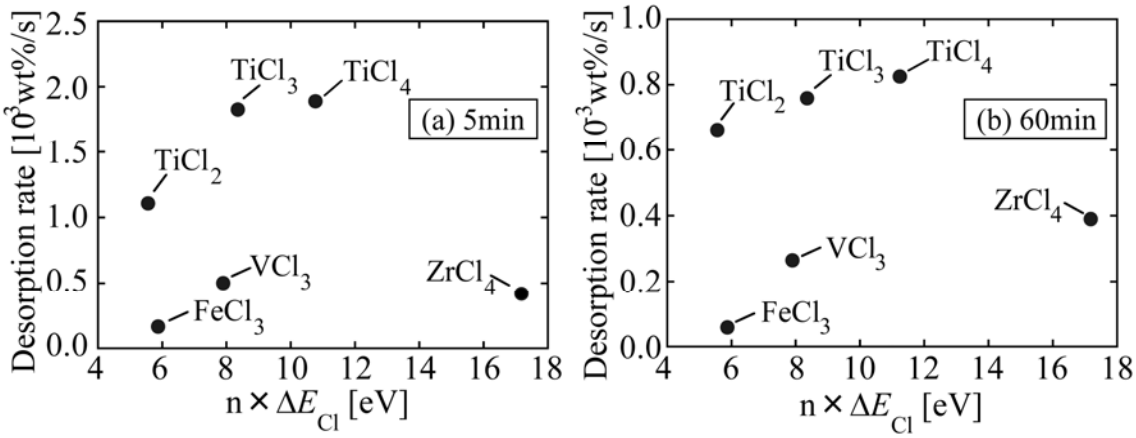

Fig. 5-4. $n \times \Delta E_{Cl}$ vs. desorption rate of $NaAlH_4$ with 2mol% metal chloride catalysts. Desorption rate is measured (a) for 0-300 sec and (b) for 0-3600 sec.

As is evident from Eqs. (1) and (2), ΔE_M and ΔE_{Cl} are defined as the values per chloride ion. However, metal chlorides, MCl_n, are added to $NaAlH_4$ by a mole unit in the experiments. So, we need to convert the values of the atomization energies per

chloride ion into the values per mole unit to compare them with the experimental data. So, each of ΔE_M and ΔE_{Cl} are multiplied by the number of chlorides ions, n, in MCl_n. The atomization energy to be counted per mole unit, MCl_n, is expressed as $n \times \Delta E_M$ for metal ions and $n \times \Delta E_{Cl}$ for chloride ions, since $n \times \Delta E_M = E_M^{atom} - E_M^{chloride}$ and $n \times \Delta E_{Cl} = \left(E_{Cl}^{atom} - E_{Cl}^{chloride}\right) \times n$, following the Eqs. (1) and (2). In other words, $n \times \Delta E_M$ and $n \times \Delta E_{Cl}$ are the energies for one M ion and n Cl ions in a MCl_n molecule, respectively.

(A) *Correlation between desorption reaction rate and atomization energy*

As shown in Fig. 5-3 (a) and (b), the addition of those metal chlorides which have large values of $n \times \Delta E_M$ tends to accelerate the hydrogen desorption reaction rate in $NaAlH_4$. Also, as shown in Fig. 5-4 (a) and (b), the addition of those metal chlorides which have large values of $n \times \Delta E_{Cl}$ may accelerate the hydrogen desorption reaction rate, although the data are rather scattered. $ZrCl_4$ seems not to conform to this attitude. It might be related to the difference of its position with other chlorides in the atomization energy diagram as shown in Fig. 5-2 but the reason still remains unknown. Both the results appear to show a positive correlation between the desorption rate and the atomization energy. This correlation, however, is clearly different from the result observed in the desorption reaction of MgH_2 with metal oxide catalysts shown in chapter 3. In case of MgH_2, the desorption reaction rate decreases with $y \times \Delta E_M$ but increases with $y \times \Delta E_O$. It is stressed here that the ions with the higher atomization energy in the catalyst will provide active reaction sites with hydrogen, resulting in the higher catalytic effect on the hydrogen desorption reaction as explained in chapter 3.

(B) *Multi-regression analysis between atomization energy and desorption rate*

In case of metal chloride catalysts, ΔE_{Cl} is comparable to ΔE_M, as shown in Fig. 5-2. So, it may be difficult to estimate which constituent element in metal chloride catalysts plays an important role in the hydrogen desorption reaction in $NaAlH_4$. To understand which element is more effective in the desorption reaction, a multiple regression analysis is performed, by assuming an equation, $[\text{desorption rate}] = A \cdot (n \times \Delta E_M) + B \cdot (n \times \Delta E_{Cl}) + C$, where A, B and C are constants to be fitted in the analysis. The results are shown in Fig. 5-5, where the calculated values are shown in the horizontal axis, and the experimental values are shown in the vertical axis. There is good agreement between them.

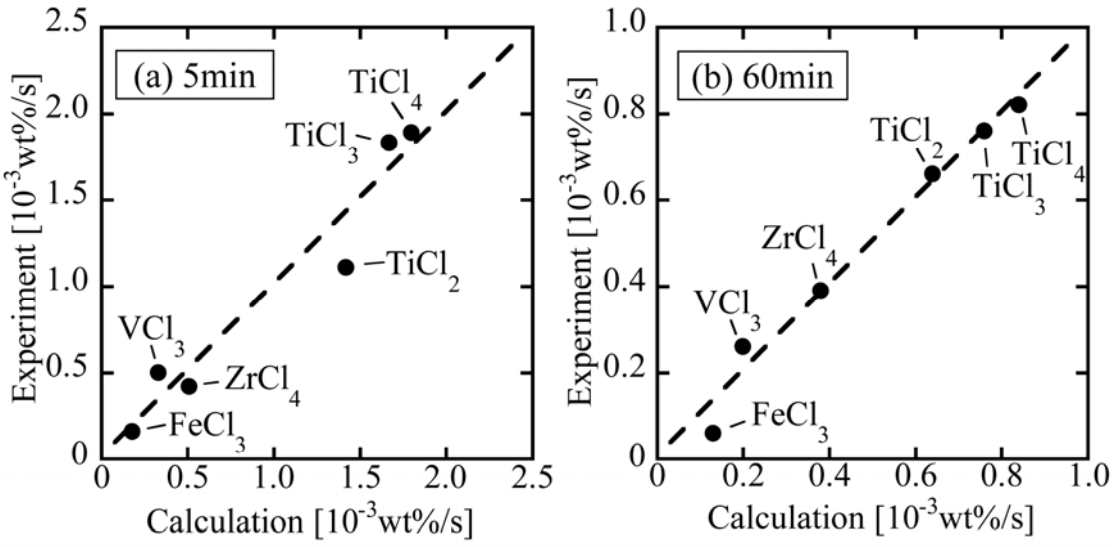

$0.273 \cdot n \times \Delta E_M - 0.001 \cdot n \times \Delta E_{Cl} - 0.349$ $0.111 \cdot n \times \Delta E_M + 0.009\ n \times \Delta E_{Cl} - 0.140$

Fig. 5-5. Multi-regression analysis between atomization energy and desorption rate of $NaAlH_4$ with metal chloride catalysts. Desorption rate data (a) for 0-300 sec and (b) for 0-3600 sec.

The value of A is much larger (Fig. 5-5 (a): A = 0.273, Fig. 5-5 (b): A = 0.111) than the value of B (Fig. 5-5 (a): B = -0.001, Fig. 5-5 (b): B = 0.009). This indicates that metal ions operate in the catalytic reaction more effectively, as compared to chloride

ions in MCl_n. Therefore, metal chlorides which have large values of $n \times \Delta E_M$ are supposed to accelerate the rate of hydrogen desorption reaction in the decomposition reaction from $NaAlH_4$ to Na_3AlH_6. For example, in case of $TiCl_3$ or $TiCl_4$, Ti works probably as a more active element than Cl in the catalytic reaction.

5.4.4 Experimental results of hydrogen desorption temperature and desorption reaction rate

The results of TDS measurement are shown in Fig. 5-6. $TiCl_3$-doped $NaAlH_4$ decomposes to Na_3AlH_6 at the lowest temperature among these three specimens. Also, Ti (nanopowder)-doped $NaAlH_4$ is found to lower the decomposition temperature, as compared to the undoped-$NaAlH_4$, indicating that Ti has indeed a catalytic effect.

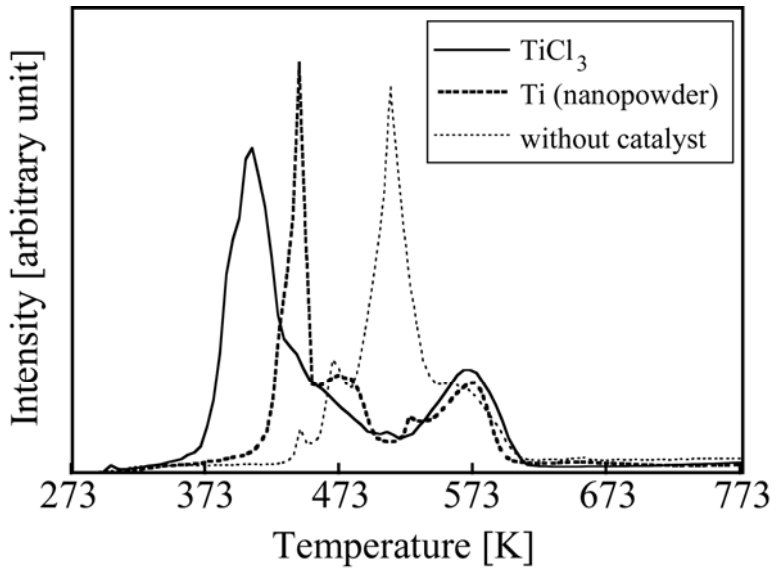

Fig. 5-6. TDS measurement for $NaAlH_4$ with and without catalysts.

The desorption reaction rate is also measured and the results are shown in Fig. 5-8. It is evident that the hydrogen desorption rate is enhanced in the order, $TiCl_3$ > TiO_2 > Ti nanopowder, indicating that the Ti cations in $TiCl_3$ or TiO_2 work to promote the catalytic

reaction more effectively than the neutral Ti atoms in Ti nanopowder. Thus, from the present experiment, it is proved that the presence of metal ions (in the present case, Ti cations) affect the hydrogen desorption reaction strongly.

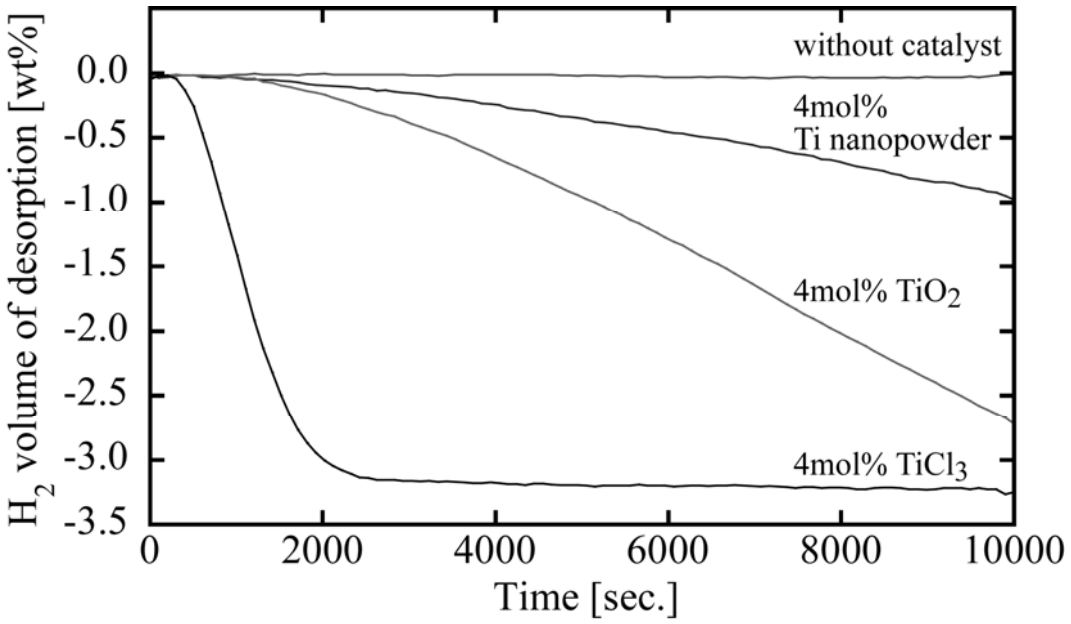

Fig. 5-8. Hydrogen desorption curves measured at 393K for $NaAlH_4$ with and without catalysts.

Also, the difference in the catalytic effect between $TiCl_3$ and TiO_2 may be attributed to the difference in the Ti cation state between them, since Ti cation state varies depending on the neighboring anion species. In this sense, anion also partially contributes to the catalytic reaction through the modification of cation states in the catalyst. However, as far as the present consideration is restricted only to the chlorides, its contribution is supposed to be small as explained in Fig. 5-5. In case of TiO_2, besides the Ti cation, the O anion may have a catalytic effect as is found in MgH_2 in chapter 3. However, judging from the relatively weak catalytic effect shown in Fig. 3-4, the O-H interaction is probably weak and hence the catalytic effect of the O anion is expected to be small in TiO_2.

5.4.5 Comparison with previous models

(A) *The function of each elements in metal chloride catalysts*

Sandrock et al. [8] reported that $TiCl_3$ decomposes during ball-milling to form NaCl and probably metallic Ti, but any final species of the Ti-catalyst formed in situ have not been precisely defined yet. Brinks et al. [9] observed the formation of NaCl and Al metal, and no titanium chlorides were detected in the hand-ground $NaAlH_4$ with $TiCl_3$ or $TiCl_4$ catalyst by means of powder X-ray diffraction. Also, it is commonly thought that chloride ion in metal chloride catalysts is inactive as a catalyst because of forming NaCl with sodium ion in $NaAlH_4$ [9, 10]. These results imply that the Ti cations yield the catalytic effect rather than chloride ions, in agreement with our result.

In addition, in Fig. 5-3, the $n \times \Delta E_M$ value for NaCl is indicated by an arrow. It is supposed from this position that NaCl does not work as a catalyst. Thus, it is apparent that the transition-metal based chlorides work as good catalysts in the hydrogen desorption reaction.

(B) *Evaluation of catalytic effect*

As shown in Fig. 5-1, Anton [3] investigated experimentally catalytic effects of various metal chlorides on the hydrogen desorption reaction of $NaAlH_4$. The difference in the catalytic effect was interpreted as due to the difference of ionic radius of cation in chlorides. Those cations which have the size lying nearly at a midpoint (0.74 Å) between the radius of Na^+ (0.97 Å) and the radius of Al^{3+} (0.51 Å) possess strong catalytic effect. The ionic radius of Ti^{3+} in $TiCl_3$ is 0.76 Å, so the maximum catalytic effect emerges in it. However, this model cannot explain the catalytic activities of $TiCl_2$

and $TiCl_4$, since their ionic radii are significantly different from the midpoint radius, 0.74 Å.

On the other hand, the present approach using the atomization energy is distinguishable in the catalytic effect among $TiCl_2$, $TiCl_3$, and $TiCl_4$, as shown in Fig. 5-3. Judging from $n \times \Delta E_M$ values, the catalytic effect changes in the order, $TiCl_2 < TiCl_3 < TiCl_4$. This is the same order as the cation charge state, $Ti^{2+} < Ti^{3+} < Ti^{4+}$. The Ti^{4+} cation in TiO_2 has the same charge state as the Ti^{4+} cation in $TiCl_4$. But, as shown in Fig. 5-8, the catalytic effect is smaller in TiO_2 than in $TiCl_3$. The $n \times \Delta E_M$ value is 6.56 eV for TiO_2 in chapter 3 and smaller than the value of about 7.4 eV for $TiCl_3$. Thus, the atomization energy approach allows us to evaluate catalytic reaction quantitatively in the decomposition process from $NaAlH_4$ to Na_3AlH_6.

5.4.6 Elemental processes of the desorption reaction in $NaAlH_4$ with metal chloride catalyst

There are two pieces of investigation in the mechanism for desorption reaction. Firstly, Baldé et al. [11] examined active Ti species in $TiCl_3$-doped $NaAlH_4$ using EXAFS and XANES spectroscopy. In the as-ball-milled fresh sample, 30% of Ti was incorporated into the surface of Al crystalline phase and 70% of Ti occupied interstitials in the $NaAlH_4$ lattice. After hydrogen desorption at 398K, $NaAlH_4$ was decomposed and the Ti-Al coordination number increased from 4.8 Al atoms to 8.5 Al atoms. They proposed that all the Ti atoms are incorporated into the surface layer of the formed Al. Thus, Ti tends to be located near Al, and sometimes makes a $TiAl_3$ cluster. Secondly, on the basis of density functional theory and phase equilibrium calculations, Bai et al. [27]

proposed that a Ti-H-Al cluster resulting from the Ti substitution of Al at the (001) subsurface layer of $NaAlH_4$ is the most stable surface defect. An interstitial H in this cluster enhances the Ti-Al bonds and weakens the Al-H bonds simultaneously. The strong Al-H bond in the $[AlH_4]^-$ complex anion in $NaAlH_4$ is weakened by the Ti-Al bond formation in a Ti-H-Al cluster. Thus, in either study, the catalytic effect of Ti emerges when the Ti-Al interaction becomes dominant. However, it is still unknown whether Ti does interact with $[AlH_4]^-$ complex anion or H or Al in $NaAlH_4$.

To understand this further, energy change is traced during the following decomposition reaction, $NaAlH_4 \rightarrow \frac{1}{3}Na_3AlH_6 + \frac{2}{3}Al + H_2$. The atomization energies of elements are listed in Table 5-2 [28]. The values in $NaAlH_4$ are counted per hydrogen atom. For comparison, the values of ΔE_{Na} and ΔE_{Al} in Na_3AlH_6 are calculated following the formulae,

$$\Delta E_{Na} = \frac{1}{4}\left(E_{Na}^{atom} - E_{Na}^{chloride}\right) ,$$

$$\Delta E_{Al} = \frac{1}{4}\left(E_{Al}^{atom} - E_{Al}^{chloride}\right) ,$$

$$\Delta E_{H} = E_{H}^{atom} - E_{H}^{chloride} .$$

Table 5-2. Atomization energies for each element in $NaAlH_4$, Na_3AlH_6, Al and H_2. (unit: eV)

	$NaAlH_4$	Na_3AlH_6	Al	H_2
ΔE_{Na}	0.11	0.35	–	–
ΔE_{Al}	-1.65	-1.94	0.85	–
ΔE_{H}	5.23	4.50	–	2.24

They are the same formulae as used in $NaAlH_4$. Also, for comparison, ΔE_{Al} for Al is

defined as one fourth of the cohesive energy of Al metal (3.39 eV). ΔE_H for H_2 is defined as a half of the binding energy of H_2 molecule (4.48 eV).

By comparing the atomization energies between $NaAlH_4$ and Na_3AlH_6, it is evident that ΔE_{Na} increases, but both ΔE_{Al} and ΔE_H decrease after decomposition. But ΔE_H values for Na_3AlH_6 is still larger than that for H_2, indicating that hydrogen is stabilized in the sodium alanate. Also, ΔE_{Al} is recovered to some extent by the separation of Al metal from $NaAlH_4$. In chapter 3, chemical interactions operating between elements are judged from the values of atomization energies for MgH_2 and Nb_2O_5 (catalyst). For MgH_2, ΔE_{Mg}= 0.38 eV, ΔE_H= 2.96 eV, and for Nb_2O_5, ΔE_{Nb}= -1.68 eV and ΔE_O= 10.99 eV. In this case, H has the higher atomization energy than Mg in MgH_2. O has the higher atomization energy than Nb in Nb_2O_5. As the element of higher atomization energy is considered to be active for the chemical reaction [29], H in MgH_2 will interact with O in Nb_2O_5. In other words, O-H interaction is dominant in the MgH_2 - Nb_2O_5 system. If similar consideration is applicable to the present $NaAlH_4$ - metal chloride system, H of the highest atomization energy in $NaAlH_4$ will interact with metal (e.g., Ti) in the catalyst. However, the desorption reaction of $NaAlH_4$ differs from that of MgH_2, $MgH_2 \rightarrow Mg + H_2$, since a $[AlH_4]^-$ complex anion in $NaAlH_4$ transforms into a $[AlH_6]^{3-}$ complex anion in Na_3AlH_6 after the hydrogen desorption. In addition, Yukawa et al. [24] have recently reported the possibility of forming a transition phase during the transformation from $NaAlH_4$ to Na_3AlH_6. Therefore, it is still not certain whether Ti interacts with H or $[AlH_4]^-$ complex anion in $NaAlH_4$.

Thus, the elementary processes between metal ions and $NaAlH_4$ are still in question. However, metal ions in the chloride catalysts play an important role in

accelerating hydrogen desorption (or decomposition) reaction rate by interacting with H or $[AlH_4]^-$ complex anion in $NaAlH_4$.

5.5 Conclusion

In order to understand the catalytic effect of metal chlorides on the decomposition reaction of $NaAlH_4$ to Na_3AlH_6, the atomization energies, ΔE_M for the metal ion and ΔE_{Cl} for the chloride ion are evaluated in various metal chlorides, MCl_n. It is found that the hydrogen desorption (or decomposition) reaction rate increases monotonously with increasing $n \times \Delta E_M$ values of metal chlorides. This indicates that the metal interacts mainly with hydrogen or $[AlH_4]^-$ complex anion in $NaAlH_4$, and the hydrogen desorption reaction on $NaAlH_4$ assists to form Na_3AlH_6, where an $[AlH_6]^{3-}$ complex anion exists. The present evaluation is the second catalyst analysis, being preceded by the first catalyst analysis of metal oxides for the hydrogen desorption reaction of MgH_2. Thus, this approach based on the atomization energy concept is applicable to various problems of catalytic reactions.

REFERENCE

[1] B. Bogdanović and M. Schwickardi, J. Alloys Compd. 253-254 (1997) 1-9.

[2] B. Bogdanović, R. A. Brand, A. Marjanović, M. Schwickardi and J. Tölle, J. Alloys Compd. 302 (2000) 36-58.

[3] D. L. Anton, J. Alloys Compd. 356-357 (2003) 400-404.

[4] B. Bogdanović, M. Felderhoff, S. Kaskel, A. Pommerin, A. Schlichte and F. Schüth, Adv. Mater. 15 (2003) 1012-1015.

[5] P. Wang, X. D. Kang and H. M. Cheng, Chemphyschem 6 (2005) 2488-2491.

[6] Y. Suttisawat, P. Rangsunvigit, B. Kitiyanan, N. Nuangsin and S. Kulprathipanja, Int. J. Hydrog. Energy 32 (2007) 1277-1285.

[7] G. J. Lee, J. H. Shim, Y. W. Cho and K. S. Lee, Int. J. Hydrog. Energy 32 (2007) 1911-1915.

[8] G. Sandrock, K. Gross and G. Thomas, J. Alloys Compd. 339 (2002) 299-308.

[9] H. W. Brinks, C. M. Jensen, S. S. Srinivasan, B. C. Hauback, D. Blanchard and K. Murphy, J. Alloys Compd. 376 (2004) 215-221.

[10] S. Singh, S. W. H. Eijt, J. Huot, W. A. Kockelmann, M. Wagemaker and F. M. Mulder, Acta Mater. 55 (2007) 5549-5557.

[11] C. P. Baldé, H. A. Stil, A. M. J. van der Eerden, K. P. de Jong and J. H. Bitter, J. Phys. Chem. 111 (2007) 2797-2802.

[12] A. Dawson, A. Parkin, S. Parsons, C. R. Pulham and A. L. C. Young, Acta Crystallogr. Sect. E.-Struct Rep. 58 (2002) i95-i97.

[13] JP. Perdew, K. Burke and Y. Wang, Phys. Rev. B 54 (1996) 16533-16539.

[14] V. Milman, B. Winkler, J. A. White, C. J. Pickard, M. C. Payne, E. V. Akhmatskaya and R. H. Noves, Int. J. Quant. Chem. 77 (2000) 895-910.

[15] D. Vanderbilt, Phys. Rev. B 41 (1990) 7892-.7895

[16] J. C. Slater, Phys. Rev. 81 (1951) 385-390.

[17] A. Schafer, H. Horn and R. Ahlrichs, J. Chem. Phys. 97 (1992) 2571-2577.

[18] S. Huzinaga, J. Andzelm, M. Klobukowski, E. Radzioandzelm, Y. Sakai and H. Tatewaki,. Gaussian Basis Sets for Molecular Calculation; Elsevier; New York, 1984.

[19] V. A. Rassolo, J. A. Pople, M. Ratner and T. L. Windus, J. Chem. Phys. 109 (1998) 1223-1229.

[20] W. J. Hehre, R. Ditchfield and J. A. Pople, J. Chem. Phys. 56 (1972) 2257-2261.

[21] T. H. Dunning, J. Chem. Phys. 90 (1989) 1007-1023.

[22] D. E. Woon and T. H. Dunning, J. Chem. Phys. 98 (1993) 1358-1371.

[23] H. Nakai, Y. Kurabayashi, M. Katouda and T. Atsumi, Chem. Phys. Lett. 438 (2007) 132-138.

[24] H. Yukawa, N. Morisaku, Y. Li, K. Komiya, R. Rong, Y. Shinzato, R. Sekine and M. Morinaga, J. Alloys Compd. 446-447 (2007) 242-247.

[25] H. Clasen, Angew. Chem. 73 (1961) 322-331.

[26] R. C. Weast, M. J. Astle and W. H. Beyer, CRC Handbook of Chemistry and Physics: A Ready-reference Book of Chemical and Physical Data (84th ed.); CRC Press; Boca Raton, 2003.

[27] K. Bai, P. S. E. Yeo and P. Wu, Chem. Mater. 20 (2008) 7539-7544.

[28] Y. Shinzato, H. Yukawa, M. Morinaga, T. Baba and H. Nakai, Adv. Quantum Chem. 54 (2008) 145-160.

[29] Y. Shinzato, H. Yukawa, M. Morinaga, T. Baba and H. Nakai, Acta. Mater. 55 (2007) 6673-6680.

Chapter 6 General conclusion

This study aims to quantitatively evaluate and understand the catalytic effect of metal oxides and metal chlorides on the hydrogen desorption reaction of MgH_2 and $NaAlH_4$ using atomization energy concept. For this purpose, geometry optimization is performed by the plane-wave pseudopotential method. The energy density analysis (EDA) is carried out in order to partition the total energy of a system into atomic energy densities of constituent elements. The atomization energy of element is defined by subtracting the atomic energy density from the energy of isolated neutral atom. The results obtained in each chapter are summarized as follows.

In chapter 1, the background and the purpose of the present study are explained.

In chapter 2, two calculation methods used in the present study are explained. One is the plane-wave pseudopotential method and the other is the energy density analysis method.

In chapter 3, in order to understand the catalytic effect of metal oxides on the hydrogen desorption reaction of MgH_2, the atomization energies, ΔE_M for the metal ion and ΔE_O for the oxide ion are evaluated in various metal oxides, MxOy. It is found that the hydrogen desorption rate increases continuously with increasing $y \times \Delta E_O$ values of metal oxide catalysts. For example, Nb_2O_5 which acts as the most effective catalyst has the highest $y \times \Delta E_O$ value (55.0 eV). On the other hand, the atomization energy of metal ions is not related to the catalytic effect of metal oxides.

This indicates that the oxide ion in MxOy interacts mainly with hydrogen atom in MgH_2, and the catalytic reaction is enhanced through the O-H interaction between them.

This is the first application of the atomization energy concept to the study of catalytic reaction of hydrogen storage material.

In chapter 4, the FT-IR spectra are measured with Nb_2O_5-catalyzed MgH_2 in order to confirm the O-H bonding operating between Nb_2O_5 and MgH_2. The absorption spectra due to the O-H stretching mode are observed experimentally in the region of 2800 to 3600 cm^{-1}, and the measured absorbance tends to decrease continuously with decreasing amount of hydrogen in the specimen. This experimental result is a direct evidence for the presence of the O-H bonding between Nb_2O_5 and MgH_2, in agreement with the prediction from the atomization energy concept.

In chapter 5, in order to understand the catalytic effect of metal chlorides on the decomposition reaction of $NaAlH_4$ to Na_3AlH_6, the atomization energies, ΔE_M for the metal ion and ΔE_{Cl} for the chloride ion are evaluated in various metal chlorides, MCl_n. It is found that the hydrogen desorption (or decomposition) reaction rate increases continuously with increasing $n \times \Delta E_M$ values of metal chlorides. For example, $TiCl_4$ which acts as the highest effective catalyst has the highest $n \times \Delta E_M$ value (7.9 eV) and $TiCl_3$ has the second highest $n \times \Delta E_M$ values (7.4 eV). This indicates that the metal in MCl_n interacts mainly with hydrogen or $[AlH_4]^-$ complex anion in $NaAlH_4$, and assists to form Na_3AlH_6, where an $[AlH_6]^{3-}$ complex anion exists. This is the second application of the atomization energy concept to the study of catalytic reaction of hydrogen storage material.

Thus, catalytic activities of metal oxides and metal chlorides are evaluated quantitatively for the first time using the atomization energy concept. This is indeed a promising approach to the finding of new catalysts. For example, it is predicted from

the calculation that SrV_3O_7 is a good catalyst for the hydrogen desorption reaction of MgH_2, because its $y \times \Delta E_O$ value is 64.0 eV, larger than the value, 55.0 eV, of Nb_2O_5.

The present study is the first application of atomization energy concept to the practical problem. This approach based on the atomization energy concept will be applicable to most of problems on catalytic reactions. For example, as explained in Chapter 3, Fe_3O_4 catalyst is used in the ammonia (NH_3) formation process (i.e., Haber-Bosch process), and this catalytic effect is understood in the same way as in the metal oxide catalysts used for the hydrogen desorption process of MgH_2. Thus, the present approach will give a new clue to the design of new catalysts in a variety of chemical reactions.

List of Paper Related to the Present Study

Chapter 3

"Quantitative Approach to the Understanding of Catalytic Effect of Metal Oxides on the Desorption Reaction of MgH_2"

H. Hirate, Y. Saito, I. Nakaya, H. Sawai, Y. Shinzato, H. Yukawa, M. Morinaga, T. Baba and H. Nakai

International Journal of Quantum Chemistry 109 (2009) 2793-2800.

Chapter 4

"Role of O-H Bonding in Catalytic Activity of Nb_2O_5 during the Course of Dehydrogenation of MgH_2"

H. Hirate, H. Sawai, H. Yukawa and M. Morinaga

International Journal of Quantum Chemistry, in press, DOI 10.1002/qua.22544.

Chapter 5

"Quantitative Evaluation of Catalytic Effect of Metal Chlorides on the Decomposition Reaction of $NaAlH_4$"

H. Hirate, Y. Saito, I. Nakaya, H. Sawai, Y. Shinzato, H. Yukawa, M. Morinaga, T. Baba and H. Nakai

International Journal of Quantum Chemistry, in press, DOI 10.1002/qua.22459.

Acknowledgments

I express my sincere thanks to many people who have helped me over this period. Above all, I would like to thank Professor Masahiko Morinaga for supervising and encouraging me throughout my research. In particular, I am indebted to Associate Professor Yoshinori Murata, Associate Professor Yoshihiro Terada and Assistant Professor Hiroshi Yukawa of Nagoya University for their valuable help and advice. Also, I would like to thank Professor Hiromi Nakai of Waseda University and Associate Professor Tomoko Yoshida of Nagoya University. I sincerely acknowledge valuable advice and comment on the thesis given by Professor Kunihito Koumoto and Professor Masataka Hiraide of Nagoya University. I will remember my co-workers in this research with great affection. In particular, I am indebted to Mr. Yasutoshi Sasaki for his kind help.

Furthermore, I would like to thank all the staff at the Materials Design Laboratory for providing me such a pleasant place to work. I owe it to Ms. Shoko Samma, who has helped me in many occasions.

Finally I would like to thank my parents and my brother for their unfailing support.

Nagoya, January 2010

Hiroshi Hirate